TITLE: CHARACTERIZATION OF MAGNETIC TAPE USING ADVANCED ANALYTICAL TECHNIQUES

by

James M. Vonick

A thesis submitted to the Faculty and the Board of Trustees of the Colorado School of Mines in partial fulfillment of the requirements for the degree of Master of Science (Materials Science).

Golden, Colorado

Date April 10, 1992

Signed: James M. Vonick
James M. Vonick

Approved: Kent J. Voorhees
Dr. Kent J. Voorhees
Thesis Advisor

Golden, Colorado

Date 10 APRIL 1992

William D. Copeland
Dr. William D. Copeland
Associate Professor and Head,
Materials Science Department

ABSTRACT

The major components of four commercial computer tapes were characterized by a variety of analytical techniques. Each tape was made by a different manufacturer. Lubricant was extracted from samples of each tape using Freon TF and analyzed by gas chromatography (GC) with both vapor phase Fourier transform infrared (FTIR) spectroscopy and mass spectrometry (MS). The lubricants from all four tapes were determined to contain fatty acids and fatty acid esters. The lubricants from two of the four tapes also contained a difunctional ester.

Electron spectroscopy for chemical analysis (ESCA) provided evidence that the magnetic coating contained chromium dioxide (CrO_2) and organic compounds. Scanning electron microscopy (SEM) indicated that the coating consisted of highly oriented acicular chromium-oxygen rich particles.

Analysis of the base films from the four tapes by FTIR spectroscopy indicated that polyethylene terephthalate was used exclusively. The crystallization and melting transitions of the four base films were detected by

differential scanning calorimetry (DSC), thermomechanical analysis (TMA) and dynamic mechanical analysis (DMA). The glass transition of the base films, however, was detected only by DSC and DMA.

Through the use of gravimetric methods, it was possible to approximate the relative percentages of base film and chromium dioxide in each tape. Determining the percentage of CrO_2 by thermogravimetric analysis (TGA) required the incorporation of a correction factor to account for the loss of oxygen during the TGA experiments.

The binders were extracted from samples of each tape using acetone and determined by FTIR spectroscopy to be polyester-polyurethanes. DMA was used to detect a physical state transition associated with the binder. This transition was suggested to be associated with the melting of the polyester soft segments. Analysis of the binder by DMA required the development of a new method capable of obtaining repeatable data on actual tape samples. The resulting data is of value to manufacturers of tape storage devices and manufacturers of magnetic tape.

TABLE OF CONTENTS

Page

ACKNOWLEDGEMENT

I would like to thank Storage Technology Corporation and Dr. Frances Planinsek for their fervent belief that higher education is critical to the development of new technologies. I would also like to thank the support provided by my advisor, Dr. Kent Voorhees, not only with this thesis but throughout the duration of my degree program. In addition, I acknowledge the support of several colleagues for their contributions: Evelyn Ackerman, Dr. Richard Adams, Walter Nielsen, Dr. Nripendra Roy, Robert Stroud and Steven Simmons. I also appreciate the cooperation of Nicolet Instrument Corporation for their permission to use copyrighted materials. Finally, I appreciate the continuous encouragement provided by my wife Patty.

Chapter 1

INTRODUCTION

Magnetic tape is vital to the computer, video, and audio industries. It is one of the primary means for storing information because of its high capacity, its relatively permanent nature, and its versatility. In addition, magnetic tape can be easily erased and used repeatedly. Over the past 20 years, magnetic tape design and manufacture have greatly improved, and applications have expanded to various arenas demanding formats which include reels and packaged systems, such as cassettes and cartridges.

Magnetic tape is a layered structure with a base film and magnetic coating as shown in Figure 1. The magnetic coating primarily consists of three components: magnetic particles, a binder and lubricants. Specifically, a mixture of these components is coated onto the base film. The binder provides the necessary adhesion to hold the structure together (1,2). Some magnetic tapes have a back coat which may have the same composition as the front coat. This back coating reduces friction during winding operations and reduces static buildup (2,3).

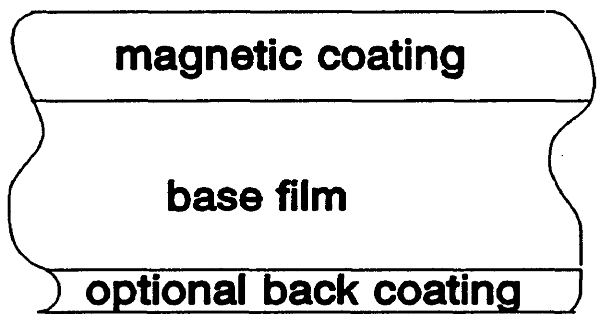

Figure 1. Schematic of magnetic tape showing both the base film and the magnetic coating.

This study characterizes the major components of four used computer tapes, one of which had a back coating. Each tape was supplied in cartridge form and made by a different manufacturer. Lubricant was extracted from samples of each tape using Freon TF and the extracted residue analyzed by gas chromatography (GC) with both vapor phase Fourier transform infrared (FTIR) spectroscopy and mass spectrometry (MS). The binder components were extracted from a second set of tape samples using acetone and the extracted residue analyzed by FTIR spectroscopy . The coating was stripped from samples of each tape so that the base films could be analyzed by FTIR spectroscopy. Electron spectroscopy for chemical analysis (ESCA) provided information about the bonding states of the magnetic particles in the coating of each tape. Scanning electron microscopy (SEM) documented the morphology of the surface features of the magnetic particles. Gravimetric techniques were used to determine the relative quantities of the major components in the tape. Three different thermal analysis techniques, differential scanning calorimetry (DSC), thermomechanical analysis (TMA) and dynamic mechanical analysis (DMA), were employed to characterize the physical states and thermal transitions associated with the base film and binder. In order to analyze the tape by TMA and DMA, methods had to first be developed that would provide meaningful and consistent results.

In this study, particular attention was paid to the tape binder because of its significant role in the performance of magnetic tape. Although DSC and DMA studies have been performed on tape binders that were cast from solution as free films (4,5), they do not provide specific information about the binders used by each magnetic tape manufacturer. Information concerning studies performed on actual production tapes is limited.

End users of magnetic tape rarely have the individual tape components readily available for examination. This luxury is afforded only to tape manufacturers because of proprietary issues. Thus, characterization techniques must be performed on the tape itself.

Of immediate concern to tape recording and storage equipment manufacturers is understanding the behavior and limitations of magnetic tape. This includes not only the electromagnetic response of the tape, but also its physical and mechanical properties. Such an understanding begins with the individual components of the tape and culminates with the final composite structure.

The ability to characterize the major components in magnetic tape serves three main purposes to manufacturers of tape recording and storage systems. First, understanding the behavior of magnetic tape is critical for establishing the design criteria for tape head assemblies. Second, timely recognition of advances in magnetic tape design can provide a competitive edge in the development of new storage and retrieval technologies. Finally, a greater level of understanding can be provided to equipment manufacturers by performing a characterization of those magnetic tapes associated with the failure of a tape head assembly .

The remainder of the Introduction provides background information on pertinent topics. First, the components used in magnetic tape are described with particular detail given to the base film and binder system. Next, key characteristics and problems associated with binder systems are reviewed with specific attention to stiction and binder degradation. Since the binder and base film are polymeric materials, physical states and transitions associated with polymers are summarized. The thermodynamics involved with these transitions are reviewed. Finally, the theory behind the operation of DSC, TMA, and DMA is discussed.

1.1 Magnetic Tape Components

Various oxides and metallic particles have been used over the years as the magnetic layer (1,2,6). Typical oxides include ferric oxide (Fe_3O_4), gamma ferric oxide (γFe_2O_3), doped iron oxides, and chromium dioxide (CrO_2). When metallic particles are used, they usually consist of elemental iron, cobalt, and/or nickel (7,8).

Today, the base film for magnetic tapes is almost exclusively polyethylene terephthalate (PET) (1,2,8,9). PET combines the mechanical strength required of a thin base film with the flexibility needed for intimate head-to-tape contact. Because of its significant role in this study, PET base films are discussed in more detail in section 1.2.

The binder is the organic polymer that holds the magnetic particles together in an immobile yet flexible matrix and adheres this matrix to the base film. Because of the demands on the flexible magnetic tape imposed by the recording device, tape binders are usually thermoplastic elastomers. That is, these binders are rubbery materials that can be melted and cooled reversibly without major changes in their chemical or physical properties. Currently, polyester-polyurethanes are the most widely used binders for magnetic tapes (1,2,5,6). Because of its significant role in this study, polyester-polyurethane binder systems are discussed in more detail in section 1.3. Carbon black (graphite) is sometimes added to the binder system to reduce electrical resistance, thereby preventing the build-up of electrostatic charges (1,2,7).

Lubricants are incorporated in most tape formulations primarily to serve two functions. The first is to minimize the friction between the head and tape. The second is to aid in the prevention of the build-up of polymeric binder particles on the head surface. A wide variety of substances have been used including fatty acids and esters, silanes, glyceryl esters, fatty acid amides, fluorinated hydrocarbons, and silica (1,2,6). Recently abrasive particles, such as aluminum oxide, have been added to magnetic coatings in very small quantities to aid in the removal of debris build-up on tape heads (1,2,6).

Solvents are used to dissolve the binder so that the magnetic particles can be dispersed and applied to the base film. Upon coating the base film, the solvent must be evaporated. It is desired that this process leave a stress free polymer structure that is well bonded to the base film. Some solvents that have been used in the manufacture of magnetic tapes include tetrahydrofuran, cyclohexanone, methyl ethyl ketone, and toluene (1,2).

Tape performance depends on the dispersion of the magnetic particles throughout the binder system. Therefore, dispersants are added to aid in the reduction of magnetic particle agglomeration. One of the common dispersants added is lecithin (1,2).

1.2 Polyethylene Terephthalate Base Films

As previously mentioned, polyethylene terephthalate is typically used as the base film in computer tape. PET is a condensation polymer with the following repeating unit (9,10):

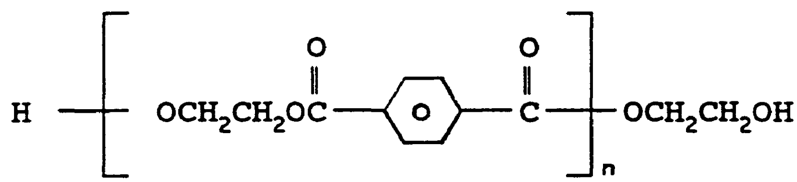

Industrial production of PET by two different polymerization processes has been described (9,10). It is made from approximately equimolar amounts of ethylene glycol and terephthalic acid or dimethyl terephthalate, depending upon the polymerization process.

PET is a semi-crystalline polymer, whose molecular structure is often described by the fringed-micelle model (10). In that model, the polymer exists as a two phase system of interconnected crystalline and amorphous domains. The manner in which these domains are distributed is a direct result of the stresses applied and the temperatures used during processing. The physical and mechanical properties of PET depend on the percentage of the structure existing in crystalline domains and the direction of the molecular chain and crystal axes.

Unless subjected to a multistep thermomechanical treatment, PET is relatively brittle and weak. The details involved in the manufacture of PET for use as a film by extrusion and biaxial stretching processes have been described (1,9,10). Molten PET is extruded through a slot die and rapidly quenched onto a chilled casting drum, so that the polymer resides in an amorphous state. Next, the amorphous sheet is reheated to about 20°C above its glass transition temperature of approximately 70°C. At this temperature, the polymer molecules gain sufficient thermal energy to have mobility. The film can be drawn by a factor of 3 to 4 in the machine direction. Structural stresses created by the drawing process causes some of the molecular chain segments to be aligned in the direction of the applied stress. This step induces crystallization with the chain axes of the crystals oriented in the machine direction. The plane of aromatic rings (100 crystal plane) tends to be oriented parallel with the film surface. At this point approximately 10 to 20% of the structure is in the crystalline phase.

The film is then reheated to approximately 100°C to enhance molecular mobility. The film is then drawn in the transverse direction, which tends to align those molecular chain segments not already aligned in the machine direction. Some of the crystallites in the machine direction are also realigned toward the transverse direction. This operation induces further crystallization. At this stage in the process, the film is capable of shrinking when exposed to temperatures above 100°C.

Finally, the film is heated between 150 to 220°C for several seconds while under restraint. In this step, amorphous chains relax, partial melting and recrystallization occur, and additional crystallites develop. This yields a clear film with a tensile strength as high as 30,000 pounds per square inch (psi). The final range of crystallinity is between 30 and 50%. The resulting structure is stable up to about 150°C.

1.3 Polyester-Polyurethane Binders

Polyester-polyurethane binders are currently the most widely used binders for magnetic tapes (1,2,5). The chemistry of polyester-polyurethanes has been examined extensively (11,12,13). These thermoplastic elastomers are linear block copolymers of the type $(AB)_n$. They contain a flexible, relatively low melting portion (soft segment) connected to a more rigid, relatively high melting portion (hard segment).

The soft segment is the polyester portion, which is composed of a repeating series of ester-linked units. The polyester segments are formed by a step-wise polymerization reaction of a difunctional carboxylic acid with a difunctional alcohol such that the ester is substantially terminated with alcohol end groups, as shown below (11,12,13).

$$\underset{\text{(carboxylic acid)}}{HO-\overset{\overset{O}{\|}}{C}-R-\overset{\overset{O}{\|}}{C}-OH} \quad + \quad \underset{\text{(glycol)}}{HO-R'-OH} \longrightarrow$$

$$\underset{\text{(polyester)}}{HO-[\overset{\overset{O}{\|}}{C}-R-\overset{\overset{O}{\|}}{C}-O-R'-O-\overset{\overset{O}{\|}}{C}-R-\overset{\overset{O}{\|}}{C}-O-R']_n-OH}$$

Increasing the chain length of the soft segment produces an increase in the elasticity of the polyurethane. The structure and chemical composition of the soft segment play a significant role in the solubility and performance of the binder, as well as dictating the binder's degradation resistance. In general, it is the soft-segment of the polyester-polyurethane that determines the low temperature and elastomeric properties of the tape (12,14).

The hard segment of the polyester-polyurethane is the polyurethane portion. As shown below, the polyurethane portion is commonly made in a reaction of almost equal amounts of a glycol and a diisocyanate (11,12,13).

$$\underset{\text{(diisocyanate)}}{O{=}C{=}N{-}R'{-}N{=}C{=}O} \quad + \quad \underset{\text{(glycol)}}{HO{-}R{-}OH} \longrightarrow$$

$$HO{-}R{-}[O{-}\overset{\overset{O}{\|}}{C}{-}\overset{\overset{H}{|}}{N}{-}R'{-}\overset{\overset{H}{|}}{N}{-}\overset{\overset{O}{\|}}{C}{-}O{-}R]_n{-}O{-}\overset{\overset{O}{\|}}{C}{-}\overset{\overset{H}{|}}{N}{-}R'{-}N{=}C{=}O$$

(polyurethane)

Many tape binder hard segments consist of a difunctional aromatic diisocyanate, such as 4,4'-diphenylmethane diisocyanate (MDI), which is reacted with a difunctional alcohol, such as 1,4-butanediol (5,6,15).

(MDI) (1,4-butanediol)

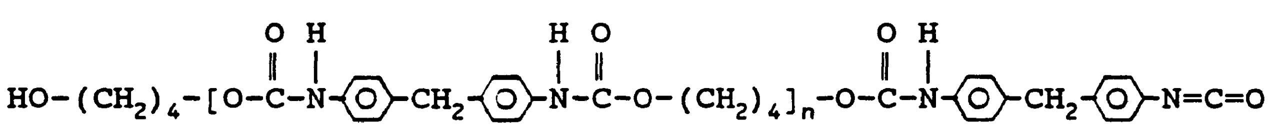

(polyurethane hard segment)

The binder's hard segments possess markedly different chemical and mechanical behavior from that exhibited by the polyester soft segments. The hard segment is a more rigid polymer with a melting point near 200°C. Compared to the soft segment in magnetic tape binders, the hard segment chain length is relatively short. This is because the hard segment has poor solubility in the solvents typically used in the manufacture of magnetic tape. In addition, an increase in the size of the hard segment blocks increases the hardness and modulus of the binder at the expense of elasticity and toughness (5,15,16).

The association of the hard segments involves strong hydrogen and dipole-dipole interactions. It has been suggested that these interactions give cohesive energies between urethane groups greater than 35.6 kiloJoules per mole (kJ/mole) as compared to 12.1 kJ/mole for the ester groups of the polyester segment (17). This results in the observed higher thermal stability of the hard segments and the aggregation of the hard segments into domains within the polyester-polyurethane. The separation of the hard segment into crystalline domains surrounded by the soft segment phase gives rise to the physical and mechanical properties of these elastomers (5).

1.4 Binder Characteristics and Associated Problems

The binder system must have several fundamental characteristics for manufacturability and for proper operation of the magnetic tape in a tape drive. First, the binder must be soluble in a solvent so that the magnetic particles can be uniformly dispersed. After the binder has solidified on the backing material, the magnetic particles must remain dispersed throughout the coating (1).

Secondly, the binder must provide the necessary adhesion to the base film. Adhesion requirements are included in an American National Standards Institute (ANSI) specification for computer tape supplied in cartridge form (18). This document specifies that the force required to peel the coating from the base film shall not be less than 1.5 newtons (5.4 ounces).

The binder must endure a large number of passes over a tape head. Ideally, it must have enough internal strength to hold the magnetic coating together without the loss of particles due to wear. It must also have enough elasticity to allow the magnetic tape to remain flexible, in order to maintain intimate head-to-tape contact.

For high density, high resolution recording, a close proximity between the magnetic tape and the head is essential. Therefore, a low flying height is maintained at the head-tape interface at high speeds. The relative speed of computer tapes during normal operation is in the order of 75 inches per second (IPS). High speed rewind is in the order of 225 IPS. At such high speeds, localized heat can be generated by friction which can cause a breakdown of the coating. In addition, during start-stop operations in a tape drive there is physical contact between the head and the tape. This contact may result in high friction which can generate high temperatures in the contact area between the head and the tape. Therefore, it is desirable that the binder exhibit good thermal stability (1,3).

Several common problems that interfere with the performance of magnetic tape stem directly from the characteristics of the binder system. Binder systems that are too rigid may result in coatings with residual stresses and poor adhesion to the base film. A binder system that is too soft and tacky may cause the tape to stick or permit easy transfer of coating debris to the tape head. Soft coatings deform more readily due to compressive stresses during operation (6). This can smooth the coating thereby increasing the real area in contact with the head. The increased contact area can produce increased friction resulting in higher wear. Thus, transfer of coating debris to the tape head can occur more readily.

Degradation studies have indicated that the PET base film is affected by moisture, but to a much lesser degree than the binder (9). Thus, any losses in physical or mechanical properties of magnetic tape caused by degradation are typically due to the binder system rather than the instability of the base film.

The transfer of coating material to tape heads is a catastrophic problem and is associated with a phenomenon called stiction. Tape stiction and an associated problem, binder degradation, are therefore discussed in further detail.

1.5 Stiction Theory

Stiction is a term used to describe the condition when the force required to initiate movement at the head-tape interface exceeds that which is expected. Stiction requires a measurable normal force to pull the two surfaces apart (3, 6). This is not to be confused with friction, which requires a tangential force to initiate sliding when two bodies are loaded together.

Loose particles can accumulate on the tape surface, due to wear of the magnetic tape over an extended period of time. This accumulation can cause an increase in the adhesive interaction between the tape and head. Because of the strong chemical bonding between surfaces in contact, stiction often results in the transfer of debris from the magnetic tape to the head. Debris build-up on tape heads results in even greater sticking causing additional transfer of material from the tape (1,3,6).

The following is a summary of stiction as theorized by Bradshaw and Bhushan (3,6). Stiction is caused by strong covalent or electrostatic bonds at the interface. Electrostatic bonds consist of at least five types of atomic interactions covering a wide range of bond strengths. These classes in decreasing order of bond strength are: ion-ion, ion-dipole, ion-induced dipole, dipole-dipole, and dipole-induced dipole. The actual transfer of polymeric debris to the metal oxide surface of the recording head usually involves ion-dipole or ion-induced dipole electrostatic bonds and thus gives rise to relatively strong adhesive interactions. The polymer-to-polymer interactions, on the other hand, generally involve the weaker dipole-dipole or dipole-induced dipole electrostatic bonds. Thus, the weaker adhesive interaction between the surfaces of a polymer-polymer contact relative to the polymer-metal surfaces permit the transfer of loose particles from the tape media to the head.

In industry, which is the test bed for many of these theories, no one mechanism has been ascribed to stiction. This phenomenon manifests itself in a variety of observable behaviors. Stiction can result in the failure of the tape to properly move across the head. The symptoms of this behavior are errors in data recovery, irregular motions of the tape, and motion aborts during restarts. In severe cases, adhesive stick can cause the removal of magnetic coating from the base film or cause physical damage to the tape (1,3,6,19).

1.6 Binder Degradation

Degradation of the polymeric binder can result in the migration of the degradation products to the surface of the tape (1,3,6,19). Such migration can produce changes in the interaction between the tape and the tape head and can result in changes in the adhesive forces between the tape and head. Severe cases of degradation can cause tape stiction.

Because of the popularity of polyester-polyurethanes for use as binders in magnetic tapes, various studies on the degradation of these materials have been performed (3,6,19,20). Polyesters, regardless of form, are subjected to the same degradative mechanism, hydrolysis. Hydrolysis involves the cleavage of the polyester chain by the addition of water to the ester linkages. This reaction produces alcohol and acid functional fragments, with a reduction in the molecular weight of the parent polymer.

Binder degradation requires a humid environment and is accelerated by elevated temperatures. The reduction in molecular weight of the binder affects the coatings ability to remain as a cohesive unit. Such degradation can cause a deterioration of the physical and mechanical properties of the tape. Temperature and humidity have also been found to be major parameters governing the frictional properties of some magnetic tapes (3,6).

In addition, the literature indicates that the low molecular weight degradation products can migrate to the surface of the tape (3). The increased polarity of the alcohol and acid functional fragments increases the attractive interaction between the coating and any mating surfaces in the tape drive. The acid-base interaction of these functional groups with metal oxides can produce strong electrostatic bonds, either ion-ion or ion-dipole. If the interaction occurs with the metal oxides in the coating, these degradation products may be immobilized. Interaction with magnetic particles, however, is sometimes hindered by prior adsorption of dispersant or components in the coating. Under these circumstances, the degradation products are free to migrate to the tape surface causing contamination. The polar interaction can then interact with metal oxides from the drive components further enhancing stiction.

1.7 Polymer States and Transitions

In order to examine the behavior of magnetic tape as a function of temperature, the physical states with which polymers can reside must be understood. Polymers exist in a variety of physical states that are temperature dependent. Of these, three extreme conditions are possible (21,22,23). In a polymer melt the molecules are free to rotate or move with respect to each other. As a glass, the polymer molecules exist in a disordered, entangled state. In this glassy state, energy barriers exist that prevent the polymer molecules from rotating or moving with respect to each other. Finally, the intermolecular attractive forces may stabilize the polymer chains so that the molecules exist in a lattice with long-range order. This latter is the crystalline state.

Crystallinity in polymers is never perfect, so that amorphous portions exist within crystalline polymers.

Completely amorphous polymers in which the polymer molecules have no crystalline form, however, do exist. The amorphous portion of a polymer may exist as a melt, glass, or some in-between rubbery state (21,22).

Three major transitions are associated with these polymer states: the melting temperature (T_m), the crystallization temperature (T_c), and the glass transition temperature (T_g). Those polymers which crystallize to any extent have a melting temperature (T_m). T_m is the highest temperature at which a crystal lattice is stable. Instead of a specific melting point, polymers typically have a melting range because a single specimen consists of various molecular weights and crystal sizes (21,22).

T_c is that temperature at which crystallization occurs. As with melting, polymers typically have a crystallization temperature range due to variations in molecular weight and crystal size.

The glass transition temperature (T_g) is the primary characteristic temperature between the amorphous solid and liquid states. An amorphous solid becomes a liquid upon heating through T_g. The glass transition temperature is that temperature at which segmental motion begins in the amorphous phase of a linear polymer. Below the glass transition temperature, amorphous polymers exist as hard, rigid glasses because of intramolecular barriers. In this glassy region, the thermal energy is too low for translational and rotational motions of segments to occur. Above T_g, the hardness of amorphous polymers decreases and flexibility increases. Segmental motion occurs. This segmental mobility is highly dependent on chain stiffness, molecular weight, and to a lesser extent on intermolecular forces. As the temperature increases above the onset of segmental motion, the intensity of the motion increases (21,22,24).

1.8 Thermodynamics of Phase Transitions

Thermodynamics provides the basis for determining phase transitions in materials. Therefore, the following is a brief review of thermodynamics as it relates to polymer states.

In thermodynamics the Gibbs free energy, G, is defined as:

$$\Delta G \equiv \Delta H - T\Delta S \qquad (1)$$

where H is the enthalpy, T is the temperature, and S is the entropy (25). A first order transition is one in which the free energy, as a function of a given state variable (volume

V, pressure p, or T), is continuous, except at the transition temperature. At the transition temperature the free energy experiences a break, such that the first derivative of the free energy with respect to the given state variable is discontinuous. This is exemplified by the following three equations:

$$(\partial G/\partial T)_p = -S \tag{2}$$

$$(\partial G/\partial p)_T = V \tag{3}$$

$$\left[\frac{\partial(G/T)}{\partial(1/T)}\right]_p = H \tag{4}$$

Thus, a first order transition has a discontinuity in entropy, volume, and enthalpy at the transition temperature (22,23,25).

Melting is a first order transition. The melting of a polymer involves an increase in disorder, and therefore an increase in entropy. A volume increase is also associated with the melting of a polymer. Third, there is a change in enthalpy or heat of fusion (H_f) associated with melting. Specifically, melting is an endothermic process. That is upon heating, when the melting point is reached, the heat of fusion has to be supplied before the temperature can rise any further (22,23,25).

At the melting temperature, both the solid and liquid phases coexist so that ΔG equals zero. Thus, from **equation 1** the following equation can be written for the equilibrium melting temperature:

$$T_m = \Delta H_f/\Delta S_f \qquad (5)$$

where ΔH_f is the heat of fusion and ΔS_f the entropy of fusion (22).

Crystallization is also a first order transition. The crystallization of a polymer involves an increase in order, and therefore a decrease in entropy. Upon crystallization of a polymer, a decease in volume is associated with this increase in order. Finally, there is a change in enthalpy associated with crystallization. Crystallization proceeds with the evolution of heat. Such a transition is an exothermic process. Upon cooling a polymer, heat is liberated in the sample at the onset of crystallization, causing a delay in the cooling. Upon the completion of crystallization, the original cooling rate within the sample is resumed (23).

For second order transitions, discontinuities appear in the second derivative of G, such as:

$$(\partial^2 G/\partial p \partial T) = V\alpha \tag{6}$$

$$(\partial^2 G/\partial T^2) = -C_p/T \tag{7}$$

where α is the volume thermal expansivity and C_p is the heat capacity at constant pressure (22,23,25).

The volume thermal expansion coefficient of a substance is defined as (25):

$$\alpha \equiv 1/V \, (\partial V/\partial T)_p \tag{8}$$

Heat capacity, C, refers to the amount of heat (dQ) absorbed by a system which undergoes a temperature change (dT) (25):

$$C = dQ/dT \tag{9}$$

Thermodynamics tells us that for a closed system with constant composition at constant pressure for a solid (25):

$$(dQ/dT)_p = (\partial H/\partial T)_p \tag{10}$$

Thus, C_p is (25):

$$C_p = (DQ/dT)_p = (\partial H/\partial T)_p \tag{11}$$

The T_g is considered to be a second order transition per **equations 6** and **7**. There are jumps in the thermal expansivity and heat capacity, but no indication of a heat of transition or an entropy of transition.

At T_g the thermal expansion coefficient (α) of the amorphous material undergoes an abrupt change. Above T_g, α has the magnitude generally associated with liquids. As the temperature decreases, a major reduction in the free volume occurs, which is made possible by configurational adjustments. Eventually, the free volume becomes so small that additional adjustments become very slow or impossible (24).

Polymers may have more than one discontinuity in α. The greatest change is usually associated with the loss of molecular mobility which permits configurational rearrangements of the chain backbones. The viscoelastic behavior of the material is profoundly altered. This is the glass transition. Other discontinuities in α may be associated with the loss of more specific local motions, such as rearrangements of short side groups (24).

Upon heating an amorphous polymer, the heat capacity also undergoes an abrupt change as it goes through its T_g. The amount of heat (dQ) absorbed by the material typically increases through this temperature change (dT).

1.9 Thermal Techniques for Analyzing Polymer Phase Transitions

Three thermal analysis techniques that provide information concerning the physical states and transitions associated with polymers are differential scanning calorimetry (DSC), thermomechanical analysis (TMA) and dynamic mechanical analysis (DMA). The remaining discussions introduce the basic theory associated with each technique.

1.9.1 Differential Scanning Calorimetry Theory.

In power compensated DSC, the sample and a reference are maintained at equal temperatures throughout a controlled temperature program (23,26). That is

$$\Delta T = T_s - T_r = 0 \tag{12}$$

where T_s is the sample temperature and T_r is the reference temperature.

This is accomplished by supplying energy at varying rates to the sample and a reference so that their temperatures remain the same. Thermal transitions are detected when the energy supplied to the sample and reference are different. Such differences occur 1) when there is a change in the sample's specific heat such as at the glass transition temperature, 2) when an endothermic or exothermic event occurs, or 3) when a chemical reaction such as decomposition occurs (23,26).

Thermal transitions in the sample appear as deviations from the baseline, depending upon whether more or less energy has to be supplied to the sample relative to the reference. A DSC output plots energy supplied versus temperature. If an endothermic event occurs, the sample temperature (T_s) temporarily lags behind the reference temperature (T_r). In order to maintain equal sample and reference temperatures, the energy supplied to the sample is increased compared to the energy supplied to the reference. Therefore, endothermic responses are represented as positive peaks occurring above the baseline. If an exothermic reaction occurs, T_s temporarily exceeds T_r, resulting in an increase in the energy supplied to the reference compared to the sample. Exothermic responses are represented as negative peaks occurring below the baseline (22,23,26,27).

Figure 2 portrays a schematic of a DSC curve with examples of both an exothermic and an endothermic response.

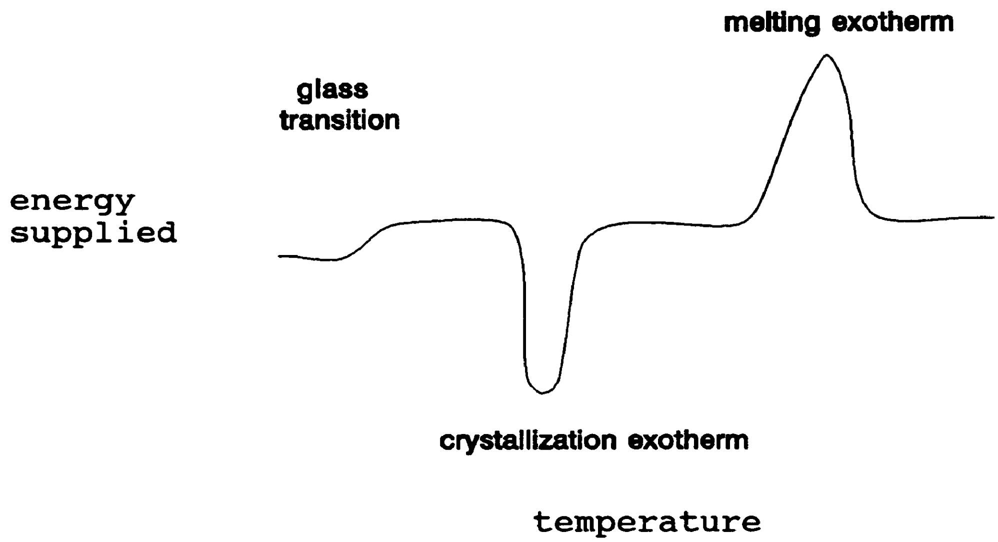

Figure 2. Schematic of the typical DSC responses. These include glass transitions, crystallization exotherms and melting endotherms.

For DSC, the area under the resulting endotherm or exotherm is directly related to the enthalpy change for a thermal event (22,27). Thus, DSC is used to analyze transitions of polymers that are accompanied by such changes.

Among its many applications, DSC can approximate the percent crystallinity of a semicrystalline polymer (23,27,28). This is done by examining the area under the melting peak, which is equal to the heat of fusion (ΔH_f) of the sample. This quantity is proportional to the percent crystallinity of the polymer. If by some means the heat of fusion, ΔH^{*}_{f}, of a hypothetical 100% crystalline sample is known, the percent crystallinity can be calculated from:

$$\% \text{ Crystallinity} = (\Delta H_f/\Delta H^{*}_{f}) \times 100 \tag{13}$$

DSC can also be used to measure heat capacities, and therefore is commonly used to determine a polymer's glass transition temperature. Recall that the glass transition, a second order reaction as defined by **equation 7**, is accompanied by a change in heat capacity, not a change in enthalpy. An example of a glass transition is included in Figure 2.

DSC curves can also be used to fingerprint a polymer by comparing the position of a peak on the temperature axis, the shape of the peak, and the number of peaks with reference curves. Since various factors, such as the heating rate and the selected purge gas, affect the resulting curve, the results are empirical in nature. Nevertheless, DSC curves are typically reproducible on a specific instrument (26,27).

1.9.2 <u>Thermomechanical Analysis Theory</u>.

TMA is a technique in which the deformation of a material is measured as a function of temperature and an applied load. Measurements can be made in several test modes including: penetration, extension, compression, flexure, and expansion.

Two types of experiments are possible. First, the deformation of a sample with an increase in the applied load is measured at a fixed temperature. This yields a stress-strain curve for a material at a specific temperature (26,27).

Secondly, the deformation of a sample with an increase in temperature is measured at a fixed load. The latter experiment yields a plot of expansion (with respect to probe position) versus temperature. From this plot the coefficient of linear thermal expansion (α_L) can be determined from the slope of the resulting expansion curve (23,27). Whereas, the thermal expansion coefficient of a substance mentioned in **equation 8** refers to a unit volume, the coefficient of linear thermal expansion corresponds to a unit length (ℓ). The two terms are related by the geometry of the sample. The coefficient of linear thermal expansion at constant stress is given by:

$$\alpha_L \equiv 1/\ell \ (\partial\ell/\partial T)_{stress} \tag{14}$$

where the stress equals the force divided by the area (23).

Glass transition temperatures, softening points, and heat distortion temperatures under load appear as discontinuities in the curve (26,27).

1.9.3 Dynamic Mechanical Analysis Theory.

The technique called dynamic mechanical analysis (DMA) is an extension of TMA. In DMA an oscillating load, typically sinusoidal, is applied to a specimen as the specimen is subjected to a controlled temperature program in a controlled atmosphere. It measures the modulus and damping of a material under oscillatory loading as a function of temperature (23,26,29,30).

The behavior of materials can be divided into three broad groups: viscous, elastic, and viscoelastic. Viscous materials, such as honey and uncured resins, deform and do not return to their original shape when a stress is applied. Elastic materials, such as steel and polymers below their T_g, deform but return to their original shape when a stress within their elastic limit is applied. Viscoelasticity is the term used to describe the behavior of materials that exhibit both elastic and viscous properties. Thermoplastics between T_g and T_m are examples of viscoelastic materials. The nature of viscoelastic behavior has been studied (24).

Studying the mechanical behavior of a material involves the application of stress to the material and examining its response. Static stress (σ) is defined as:

$$\sigma = F/A \tag{15}$$

where F is the applied force and A is the initial cross sectional area of the specimen. Strain (ϵ) is defined as the change in length (ΔL) of the specimen with respect to the original length (L) of the specimen.

$$\epsilon = \Delta L/L \tag{16}$$

The elastic modulus (E) is the stress divided by the strain:

$$E = \sigma/\epsilon \tag{17}$$

In viscoelastic studies of polymeric materials using DMA, stress is applied to a specimen periodically, typically with a sinusoidal alteration at an angular frequency of ω

(in radians/second). The stress and strain can be expressed as follows:

$$\sigma = \sigma_o \sin (\omega t + \delta) \quad (18)$$

$$\epsilon = \epsilon_o \sin \omega t \quad (19)$$

where σ_o and ϵ_o are the amplitudes of the stress and strain, and δ is the phase angle. The phase angle is defined as the amount of time it takes for the material to respond to the applied stress. For purely elastic behavior, the stress and strain are in phase so that the phase angle is 0. For purely viscous behavior, the stress and strain would theoretically be out of phase by 90° (23,30).

For viscoelastic behavior the applied force and resulting deformation both vary sinusoidally with time. The rate at which the load is applied is specified as the frequency f (in cycles per second) or ω, which equals $2\pi f$ (in radians per second). For linear viscoelastic behavior energy dissipation causes the sample strain to be out of phase with the applied force. That is, the maximum strain does not occur at the same instant as the maximum force. This phase shift or lag is the phase angle. This phase shift results from the time associated with molecular rearrangements and relaxation phenomena (26,30).

The term for stress can be rewritten as (23,30):

$$\sigma = \sigma_o \sin \omega t \cos \delta + \sigma_o \cos \omega t \sin \delta. \tag{20}$$

For viscoelastic materials the stress can be considered as the sum of two components, one term that is in-phase with the strain ($\sigma_o \cos \delta$) and one that is 90° out-of-phase ($\sigma_o \sin \delta$). This relationship is:

$$\sigma = \epsilon_o E' \sin \omega t + \epsilon_o E'' \cos \omega t \tag{21}$$

such that

$$E' = (\sigma_o/\epsilon_o) \cos \delta, \text{ and} \tag{22}$$

$$E'' = (\sigma_o/\epsilon_o) \sin \delta. \tag{23}$$

where E′ is the real part of the modulus, and E′′ is the imaginary part (23,30). This real part of the modulus is the in-phase response to a sinusoidally varying strain and is called the elastic or storage modulus. The storage modulus expresses a material's ability to store energy as potential energy and its release in the periodic deformation. The imaginary part of the modulus is the out-of-phase response and is called the viscous or loss modulus (E''). The loss modulus expresses a material's ability to dissipate mechanical energy by converting it to heat through molecular motion. The absorption of mechanical energy is often related to the movements of molecular segments within the material, such as specific molecular groups within the main polymeric chain or polymeric side group (29,30).

A complex representation of the modulus can be derived using:

$$\epsilon = \epsilon_o \exp i\omega t \tag{24}$$

$$\sigma = \sigma_o \exp i(wt + \delta) \tag{25}$$

Thus, the complex modulus (E^*) can be represented as:

$$E^* = \frac{\sigma}{\epsilon} = \frac{\sigma_o}{\epsilon_o} e^{i\delta} \tag{26}$$

$$E^* = \frac{\sigma_o}{\epsilon_o} (\cos \delta + i \sin \delta) \tag{27}$$

From **equations 22** and **23** for the storage and loss moduli, the complex modulus is defined as (23,30):

$$E^* = E' + iE'' \tag{28}$$

$$(E^*)^2 = (E')^2 + (iE'')^2 = (E')^2 + (E'')^2 \tag{29}$$

Thus,

$$E^* = [\ (E')^2 + (E'')^2\ ]^{1/2} \tag{30}$$

From **equations 22** and **23** for the terms E′ and E′′, a relationship can be derived for the phase angle (δ) as follows (23,30):

$$\frac{E''}{E'} = \frac{(\sigma_o \sin \delta)/\epsilon_o}{(\sigma_o \cos \delta)/\epsilon_o} = \tan \delta \tag{31}$$

Tan δ is measured as the tangent of the phase angle difference between the sinusoidal applied force (or stress) and the output strain of a dynamically deformed specimen. The relationship between the two (E′′/E′) is the loss tangent, or dissipation factor, commonly referred to as tan δ. A relatively high tan δ indicates viscous behavior (that is the sample is dissipating most of the energy supplied). A relatively low tan δ indicates elastic behavior (the sample is storing most of the energy supplied) (23,29,30).

As previously observed, viscoelastic materials have a complex modulus consisting of in-phase and out-of-phase elements. When a viscoelastic material is tested in the oscillatory mode at strains with small amplitudes, the two components of the complex modulus are separated. DMA detects both the storage and the loss moduli responses in viscoelastic materials. From these responses tan δ can be tracked. Tan delta and loss modulus peaks have been used to indicate the presence of phase transitions. There are several possible DMA excitation modes: extension, single cantilever, dual cantilever, compression, and three point bending (flexural) (23,26,30).

In summary, the main goal in DMA is to relate the responses to microscopic bond deformation and molecular conformational changes that originate from molecular rearrangements. These responses provide quantitative information on the elastic and viscoelastic properties of polymeric materials. Storage modulus measurements provide information on the rigidity, and therefore, the strength of a material. The loss factors (tan δ and loss modulus) provide information on transitions. The largest loss peak for an amorphous material is associated with the glass transition temperature. For highly crystalline polymers, loss peaks are associated with melting (22,23,30).

Chapter 2

INSTRUMENTATION AND PROCEDURES

Four magnetic tapes, each made by a different manufacturer, were analyzed in this study. These tapes were 1/2 inch wide computer tapes supplied in cartridge form. These tapes were designated by the letters A through D. Tapes A, B and C were single coated tapes, while Tape D was a double coated tape. All of the tapes had been previously used in computers.

The procedures are broken into two sections: 1) those techniques used to characterize the major components in the magnetic tape and 2) the three thermal analysis techniques used to examine the transition temperatures of the binder and base film in the magnetic tape.

2.1 Characterization of Major Magnetic Tape Components

Lubricant was extracted from each tape using Freon TF and the extracted residue analyzed by gas chromatography

(GC) with both vapor phase Fourier transform infrared (FTIR) spectroscopy and mass spectrometry (MS). The binder components of each tape were extracted with acetone and identified using FTIR spectroscopy. After stripping the magnetic coating off samples of each tape, each base film material was analyzed by FTIR spectroscopy. Electron spectroscopy for chemical analysis (ESCA) was used to provide chemical state information of the magnetic particles in the tape coatings. Scanning electron microscopy (SEM) documented the morphology of the surface features of the magnetic particles. Gravimetric techniques, including thermogravimetric analysis (TGA), were used to determine the relative quantities of the major components in the tape. Table 1 below summarizes the techniques used to characterize the major tape components.

Table 1

Characterization Technique Summary

Tape Component	Technique
1) Lubricants (Freon soluble residue)	GC/FTIR/MS
2) Binder (acetone soluble residue)	FTIR
3) Base Film	FTIR; Gravimetric
4) Magnetic Coating	ESCA; SEM
5) Entire Tape	Gravimetric

2.1.1 Freon TF Extraction Procedure.

An extraction process using Freon TF was used to remove lubricant from each tape. Four 400 milliliter (ml) beakers, previously cleaned with Micro[1], were rinsed with acetone and then with distilled Freon TF. A section of tape, measuring approximately 96 inches, was cut from each tape cartridge and placed into individual beakers. The samples were submerged in 200 ml of distilled Freon TF and allowed to soak for eight hours. Afterwards, the tape samples were removed from the beakers and the solvent allowed to evaporate over night. On the following day, the residue in each beaker was redissolved using a few ml of distilled Freon TF and transferred to 2 ml chromatographic sample vials. These vials were then placed onto a hot plate to facilitate evaporation of the solvent. The vials were capped with crimp-top septa. A syringe was used to inject 30 microliters of distilled Freon TF into each vial. Each residue was then analyzed by gas chromatography.

[1]Micro is distributed by Cole-Parmer Instrument Company. It is a phosphate free cleaning agent that contains sodium, ammonia, triethanolamine, ethylenediaminetetraacetate, linear alkylarylsulfonates, polyethoxynonylphenol, and water.

2.1.2 GC/FTIR/MS Analysis of Freon Soluble Residues.

The freon soluble residues from each tape were individually analyzed by high resolution GC with both vapor phase FTIR spectroscopy and MS. GC and accompanying detectors are used to separate, isolate, and identify components of mixtures. GC is based on differences in rates at which the individual components of a mixture migrate through a stationary phase while under the influence of a mobile phase. High resolution gas chromatography uses open tubular capillary columns, in which the inside column wall provides solid support. The column wall is coated with a film, which acts as the stationary phase, and a gas is used as the mobile phase. A liquid sample is injected into the chromatograph where it is vaporized. Upon vaporization, the components of the mixture flow through the column at different rates depending upon their retention by the column. The spectral data generated by the detectors is used to identify the components of the chromatographic separation (31).

A Hewlett Packard 5890A gas chromatograph was used in this study. This gas chromatograph has an upper temperature limit of 275°C. The gas chromatograph was fitted with a 0.53 millimeter (mm) inner diameter, 30 meter DB-1 Megabore capillary column. The column was made from fused silica with a polyimide outer coating. The interior film on the column was dimethyl polysiloxane. The mobile or carrier phase was helium gas with a flow rate 25 ml per minute. Detection of chemical components from the extracted residue samples was accomplished first by vapor phase FTIR spectroscopy followed by MS. The FTIR detector was a Hewlett Packard 5965A and the MS detector a Hewlett Packard 5970. Perfluorotributylamine (PFTBA) was used as a calibration standard for the MS.

A 3.0 microliter aliquot of a freon extracted tape residue was injected into the GC by a direct injection (splitless) method. The GC oven was programmed from 40°C to 275°C at a rate of 15°C per minute. The output of the FTIR detector is the total response chromatograph (TRC), which plots response versus evolution time. The major peaks in the TRC were individually displayed in terms of percent transmittance over a frequency range of 800 to 4000 cm^{-1} wavenumbers so that each component could be identified. Identification of the detected compounds was performed in the absorbance mode and was facilitated using computerized library search algorithms.

The MS had a limit of 800 atomic mass units (AMU). The output of the MS detector is the total ion chromatograph (TIC), which plots abundance of a component versus evolution time. The major peaks in the TIC were individually displayed in terms of abundance versus mass/charge so that each component could be identified. Identification of the detected compounds was also facilitated through the use of computerized library search algorithms.

2.1.3 Acetone Extraction Procedure.

An extraction process using acetone was used to remove binder from each tape. Four 400 ml beakers, previously cleaned with Micro, were rinsed with acetone. A section of tape, measuring approximately 48 inches, was cut from each tape cartridge and placed into separate beakers. Each sample was submerged in 200 ml of acetone and allowed to soak for two hours. Afterwards, the tape samples were removed from the beakers and the beakers placed on a hot plate to aid in the evaporation of the solvent. The residue extracted from each tape sample was then analyzed using FTIR spectroscopy to identify the chemical constituents of the residue.

2.1.4 FTIR Analysis of Acetone Soluble Residues.

The acetone soluble residues were individually analyzed by FTIR spectroscopy. Infrared spectroscopy is used to determine the chemical functional groups contained within a particular material based on molecular vibrations. Each functional group uniquely absorbs characteristic frequencies of infrared radiation. The amount of radiation absorbed or passed through unchanged depends on the chemical composition of the sample. A plot of radiation intensity versus frequency is used to fingerprint the chemical groups in the material.

Each acetone extracted residue was individually analyzed using a Nicolet 730 FTIR spectrometer in the transmission mode with a Spectra-Tech FTIR microscope. Several drops of acetone were placed in a beaker with an acetone extracted residue in order to collect the residue in solution. The solution was deposited as a thin film on a clean silver chloride (AgCl) test cell. The cell was placed on the sample stage of the FTIR microscope which was focused on the surface of the cell. A spectrum of the residue was then generated. A blank spectrum of the AgCl cell was also gathered and electronically subtracted from the sample spectrum. The result was plotted in terms of radiation intensity (percent transmittance) versus frequency (670 to

4000 cm^{-1} wavenumbers). This spectrum was compared in the absorbance mode against a computerized library of standards to aid in the identification of the residue.

2.1.5 FTIR Analysis of Base Film Materials.

Samples of base film from each magnetic tape were also individually analyzed by FTIR spectroscopy. After stripping the magnetic coating off a sample of tape with tetrahydrofuran, the base film material was analyzed using a Nicolet 730 FTIR spectrometer in the reflectance mode with a Spectra-Tech FTIR microscope. With the aid of an optical microscope under low magnification, small particles of the tape backing material were generated by scraping the material's surface. A thin particle was removed and placed on a polished aluminum mirror. The mirror was placed on the sample stage of the FTIR microscope. The microscope was focused on the particle and a spectrum of the particle generated. A blank spectrum of the mirror was also gathered and electronically subtracted from the sample spectrum. The result was displayed in terms of radiation intensity (percent transmittance) versus frequency (670 to 4000 cm^{-1} wavenumbers). This spectrum was then compared in the absorbance mode against a library of computerized standards to aid in the identification of the material.

2.1.6 ESCA Analysis of Magnetic Coatings.

The magnetic coating of a sample from each tape was examined by the ESCA technique. ESCA is a surface technique in which the sample is irradiated with a beam of Kα X-rays from an aluminum source. The X-rays cause electrons to be emitted from molecules on the surface of the samples by the photoelectron effect. The kinetic energy of the emitted photoelectrons is measured. The binding energy of the excited electrons in the molecule is determined from the measured kinetic energy of the photoelectron. The binding energy gives chemical state (bonding) information about the materials found on the surface of the sample (32,33).

The instrument used to perform the ESCA study was a Perkin Elmer 5000LS. A survey scan was taken of each sample using a spot size of 1.1 mm diameter in order to determine the elemental composition of the sample surface. The resulting survey spectrum was displayed as the number of electrons versus the binding energy in a range of 0 to 1000 electron volts (eV). After determining the elemental composition of the sample, a multiplex spectrum was taken of the regions of interest as indicated on the survey spectrum.

2.1.7 <u>SEM Analysis of Magnetic Coating</u>.

The magnetic coating of a sample from Tape B was examined with a SEM. SEM is a technique in which the a conductive sample is bombarded with an electron beam. In general, nonconductive samples can also be examined providing a conductive coating is applied to the sample surface. Using secondary electron imaging the surface morphology can be photographically documented. Using energy dispersive spectroscopy (EDS), X-rays are generated from the sample and detected with an appropriate detector from which qualitative chemical information can be determined about the sample (34).

The instrument used to perform the SEM study was a Philips 505. A small section from Tape B, measuring approximately 1 square centimeter (cm^2), was mounted with the media side-up on a SEM stub using conductive carbon tape. The sample was examined in the "as received" condition without a conductive coating. The sample was bombarded with an electron beam using 25 kilovolts with a spot size of 100 nanometers and with a spot size of 20 nanometers. The secondary electron imaging technique was used to photographically document the morphology of the surface features. EDS was used to qualitatively determine the chemistry of the magnetic particles. The detected elements were displayed on a spectrum as intensity versus the eV energy.

2.1.8 Gravimetric Analysis of Base Films.

A gravimetric method was used to approximate the quantity of base film in each tape. Three samples from each tape, measuring approximately 3 inches long, were weighed separately using a Metler H542 analytical balance capable of measuring to ± 0.1 milligrams (mg). Afterwards, the coating on each sample was removed by wiping each with tetrahydrofuran. The samples were placed in an oven at 65°C for 30 minutes to drive off any absorbed solvent and then weighed. The base film samples were reheated at 65°C for another 30 minutes and reweighed. This procedure was repeated until the sample exhibited no weight change between consecutive readings. The weight of the base film was reported as a percentage of the original weight of the tape.

2.1.9 TGA of Base Films and Magnetic Tapes.

Samples of each tape, their base films, and a sample of DuPont chromium dioxide used in magnetic tapes were analyzed by TGA. These experiments in conjunction with the gravimetric technique in the previous procedure were used to determine the relative quantities of the major components in the tape.

The TGA is a thermal analysis technique that measures the change in sample mass, either loss or gain, as a function of temperature in a controlled atmosphere. The resulting curve is called a thermogram, which provides information about the thermal stability and composition of the test sample. The technique characterizes materials that exhibit weight changes due to decomposition, dehydration, or oxidation. Measurements are made with the thermogravimetric analyzer, which basically consists of a microbalance, a furnace, a thermocouple for monitoring the sample temperature, a purge gas port, and a temperature control system.

The TGA was performed using a Perkin-Elmer TGA 7. A weight calibration was performed using a 50 mg calibration standard. Temperature calibration was performed based on the Curie points of two magnetic standards, alumel (163°C) and perkalloy (596°C). Afterwards, a nine point furnace calibration in the range of 50°C to 900°C was performed and the chromel-alumel thermocouple temperature matched to the programmed furnace temperature (35).

Samples of the base film were obtained by removing the coating from samples of each tape with tetrahydrofuran. No less than 2 mg and no more than 5 mg of a base film material were placed in a clean, tared platinum pan. The sample size was restricted by the dimensions of the platinum pan. The pan was suspended in the furnace assembly of the TGA instrument by means of a nichrome hang-down wire, that was attached to the microbalance. The furnace assembly was purged with a continuous stream of air. After reaching thermal equilibrium the sample was weighed. The furnace was then heated from 20°C to 800°C at a rate of 10°C per minute. After completing each TGA run, the thermogram was displayed in weight % versus temperature (°C). The onset of degradation was determined for each transition and reported as a temperature in °C.

Magnetic tape samples were also analyzed by TGA. Between 1 and 3 mg of a tape sample were placed in a clean, tared platinum pan with the coated side of the tape facing away from the bottom of the pan. In the case of Tape D, which was coated on both sides, the side not used for storing data lay facing the bottom of the pan. Only one piece of tape was added to the pan in order to avoid stacking tape samples on top of each other. The sample size was determined by the diameter of the platinum pan. The pan was suspended in the furnace assembly of the TGA instrument, which was purged with a continuous stream of nitrogen and air. After reaching thermal equilibrium the sample was weighed. Three samples from each magnetic tape were analyzed in the same manner as the base film samples. After completing each TGA run, the thermogram was displayed in weight % versus temperature (°C). The onset of degradation was determined for each transition and an average of the three samples reported as a temperature in °C.

A sample of DuPont brand chromium dioxide in powder form was also analyzed by TGA. Prior to analysis, the chromium dioxide was heated in an oven for 2 hours at 66°C to drive out any moisture. A sample weighing approximately 2.5 mg was placed in a clean, tared platinum pan. The pan was suspended in the furnace assembly of the TGA instrument, which was continuously purged with a stream of nitrogen and air. After reaching thermal equilibrium, the sample was weighed. The furnace was then heated from 20°C to 800°C at a rate of 10°C per minute. After completing the TGA run, the thermogram was displayed in weight % versus temperature (°C). From this thermogram, the weight change of the chromiun dioxide that occurred during the experiment was determined.

2.2 Transition Temperature Analysis Techniques

Three techniques were used to identify the transition temperatures associated with the binder and base film in the magnetic tape: differential scanning calorimetry (DSC), thermomechanical analysis (TMA), and dynamic mechanical analysis (DMA). The basic theory of each technique was reviewed in section 1.9 of the Introduction. The primary goal for analyzing magnetic tape by these techniques was to provide physical state information about the binders used in magnetic tape. Such information could then be used when evaluating tape head failures caused by stiction and in developing media requirements for future technologies. To do this, transitions associated with the base film had to first be identified and understood. In the case of TMA and DMA methods that provide repeatable results for both the base film and binder had to be developed. Table 2 below summarizes the transition temperature techniques used to characterize the base film and the binder.

Table 2

Transition Analysis Technique Summary

Tape Component	Technique
Base Film	DSC, TMA, DMA
Magnetic Coating	DSC
Entire Tape	DSC, TMA, DMA

2.2.1 DSC Analysis of Base Films, Magnetic Tapes and Magnetic Coatings.

Several different sample types were analyzed by DSC. First, base film from each tape was analyzed. The base films were obtained by stripping the coating from each tape with tetrahydrofuran. Entire samples of each tape were also analyzed. Finally, coating was scrapped from each tape using a razor blade and analyzed.

The instrument used to perform the DSC analyses was a Perkin-Elmer Corporation DSC 7. This instrument is based on the power compensated 'null-balance' principle, in which energy absorbed or evolved by the sample is compensated by adding or subtracting an equivalent amount of electrical energy to a heater located in the sample holder. The continuous and automatic adjustment of heater power (energy per unit time) necessary to keep the sample holder temperature identical to that of the reference holder provides a varying electrical signal equivalent to the varying thermal behavior of the sample. This measurement is made directly in energy units (milliwatts), providing an electrical energy measurement of peak areas (36).

This instrument consists of several basic components. First, it contains identical low mass sample and reference holders (furnaces) constructed of a platinum-iridium alloy embedded in a large aluminum heat-sink. Each holder is a separate calorimeter with its own platinum resistance heater and temperature sensor to provide the temperature and energy measurements. Thus, the reference and sample can be heated separately as required. Any residual differences between the two calorimeters are eliminated by calibration. The system also has an insulated reservoir that allows the use of liquid nitrogen for operation at subambient temperatures (36).

The temperature and energy calibration was accomplished using high purity standard materials that have a melting transition of known temperature and energy. The temperature calibration was performed using a two-point standard calibration. The selected standards were n-decane ($CH_3(CH_2)_8CH_3$), which has a melting temperature of -29.66°C, and lead, which has a melting temperature of 327.47°C. The energy calibration was performed using a single standard, indium, which has a ΔH peak area of 28.45 (36).

Each sample was individually analyzed by DSC using the same basic procedure. First, a baseline was established. Empty aluminum pans were sealed using a crimp press and placed in both the system's sample and reference holders. The furnace was heated through a specific temperature range at a constant rate of 5°C per minute. The furnace was continuously purged with nitrogen throughout the baseline run. The energy, required to maintain the sample and the reference at the same temperature was monitored as a function of temperature. This baseline was saved in the computer's memory, and subtracted from each sample run. A new baseline was determined at the start of each day of testing.

After performing the baseline run, a sample of known weight (between 1.5 and 7 mg depending on the sample) was placed into a clean aluminum pan. The pan was sealed and placed in the DSC's sample holder. The furnace was heated in the same temperature range and at the same rate as the baseline run. The furnace assemblies were continuously purged with nitrogen throughout the analysis. The energy required to maintain the sample at the same temperature as the reference was monitored as a function of temperature.

The resulting thermogram was plotted. Locations of any transitions were identified by an onset temperature, a peak or midpoint location, and an endpoint.

The base films from each tape were analyzed over a temperature range of 25°C to 300°C. Upon completion, the sample was quenched at a cooling rate of 200°C per minute. Afterwards, the sample was rerun under the initial conditions. The percent crystallinity of the base films was determined for each run using equation 13 in section 1.9.1.

Entire tape samples and coating samples were analyzed over a temperature range of -25°C to 300°C. Upon completion, a sample was quenched at a cooling rate of 200°C per minute. Afterwards the sample was rerun under the initial conditions.

2.2.2 TMA of Base Films and Magnetic Tapes.

The TMA experiments were individually performed on both magnetic tape and base film samples. The base film samples were obtained by removing the coating from the tape with tetrahydrofuran. TMA is a technique in which the deformation of a material is measured as a function of temperature and an applied load. The TMA experiments in this study consisted of the measurement of deformation with temperature at a fixed load.

The instrument used to perform the TMA analyses was a Perkin-Elmer Corporation TMA 7. This instrument consists of three major components: a linear variable differential transformer (LVDT), a low mass furnace, and a linear motor for probe loading. With this instrument one of several probes is in contact with the sample, whose temperature is controlled by a linearized resistance thermometer in a low mass furnace. The sample temperature is monitored using a chromel-alumel thermocouple. As the sample expands, contracts, or softens, the position of the probe changes. The probe position is monitored by a linear variable differential transformer (LVDT) which provides a signal which is proportional to the probe displacement. The application of a desired force to the probe is controlled independent of probe position by a linear motor (37).

Several calibrations were necessary for the TMA. The vertical axis of the system was calibrated using a height displacement standard made of polished ceramic. A force calibration was performed with the aid of weight standards. An eigen deformation calibration determined the systems compliance and corrected the DMA data for this compliance.

This calibration was performed using a 9.5 mm thick steel sample (37).

The thermocouple temperature was calibrated using the onset of the melting points of two high purity standards, mercury (-38.84°C) and lead (327.47°C). These melting points were determined in the penetration test mode by a change in probe position. As the standard melts, the probe penetrates the standard. A linear transformation is done at all points between these two temperatures. Afterwards, a nine point furnace calibration in the range of 50°C to 600°C was performed and the chromel-alumel thermocouple temperature matched to the programmed furnace temperature (37).

The TMA measurements are possible in several test modes including: penetration, extension, compression, flexure, and expansion. The TMA tests in this study were performed in the extension mode because the samples existed in the form of thin films. Rectangular samples, measuring approximately 5 mm wide by 9 mm long, were cut using a razor blade. The base film from Tape B was analyzed using three different static loading conditions, 50, 250 and 500 millinewtons (mN). Samples of the base films from the remaining tapes were analyzed only under a 50 mN static load. The furnace, that encompassed the extension fixture with a base film sample, was heated from -25°C to 250°C at a constant rate of 5°C per minute. Each magnetic tape was also analyzed under a 50 mN static load. The furnace was heated from -25°C to 250°C at a constant rate of 5°C per minute for the magnetic tape samples. The extension fixture and furnace assembly were purged with a continuous stream of nitrogen throughout each analysis. The height of the upper extension grip (mm) was plotted versus temperature (°C) for all of the samples. The onset temperatures for each major discontinuity was calculated.

2.2.3 DMA of Base Films and Magnetic Tapes.

The DMA experiments were individually performed on both tape and base film samples. Base film samples were obtained by removing the coating from the tape with tetrahydrofuran. The instrument used to perform the dynamic mechanical analyses was a Perkin-Elmer Corporation DMA 7. It is the same instrument used to perform the TMA analyses. Its major components are described in the preceding TMA procedure section. In the case of DMA, however, the load is not fixed but applied sinusoidally. Calibration of the TMA and DMA systems is identical (38).

There are several possible DMA excitation modes: extension, single cantilever, dual cantilever, compression, and three point bending (flexural). The DMA tests in this study were performed in the extension mode. Rectangular samples, measuring approximately 5 mm wide by 9 mm long, were cut using a razor blade. In order to obtain meaningful results, the dimensions of the samples were accurately measured.

The thickness of each tape and base film was measured using a position indicator capable of reading to 0.00001 inch. The measurements were made on a clean granite surface plate. Ten measurements were taken for each tape and base film at different locations. The average of these ten measurements was taken as the thickness of the samples used in the DMA tests. The thicknesses were converted and reported in micrometers (μm). The width of each sample was measured using a Nikon stereomicroscope at an approximate magnification of 20x with a Nikon x-y stage controlled by Mitutoyo digital micrometers capable of measuring to 0.001 mm. The width of each sample was measured at three places and an average of these taken as the width. The length of each sample was determined by the DMA system as the distance between the extension grips.

Three DMA samples were cut from each tape cartridge and from samples of each base film material. A sample was mounted into the extension grips of the DMA and the furnace raised around the test area. A dynamic tensile stress of 500 mN was applied to the sample at a sinusoidal frequency of 1 hertz. The furnace was heated from -25° to 225°C at a constant rate of 5°C/minute. The extension fixture and furnace assembly were purged with a continuous stream of nitrogen throughout each analysis. The storage modulus in Pascals (Pa), loss modulus in Pa, and tangent of the phase angle (tan δ) were plotted versus temperature.

Chapter 3

RESULTS AND DISCUSSION

3.1 Characterization of the Major Tape Components

A variety of analytical techniques were used in this study: gas chromatography with both a vapor phase Fourier transform infrared detector and a mass selective detector (GC/FTIR/MS); Fourier transform infrared (FTIR) spectroscopy; electron spectroscopy for chemical analysis (ESCA); scanning electron microscopy (SEM); and gravimetric techniques, including thermogravimetric analysis (TGA). The purpose was to identify those physical characteristics of the magnetic media, binder and base film that would allow full characterization of commercial magnetic tapes and provide a basis for monitoring tape quality.

3.1.1 GC/FTIR/MS Analysis of Freon Soluble Residues.

The GC/FTIR/MS was used to identify the residues extracted with Freon from each tape. The total response chromatograph (TRC) of the infrared detector for the Freon soluble residue extracted from Tape A is shown in Figure 3, and the total ion chromatograph (TIC) of the mass spectrometry detector for the same residue is shown in Figure 4. Five major peaks were detected in the TRC for Tape A and four peaks in the TIC. Notice that the peaks in the TRC are more pronounced than the peaks in the TIC. The MS detector is less sensitive than the FTIR detector because mass spectrometry closely correlates with concentration, whereas infrared spectroscopy is related to the absorption (or extinction) coefficient. Absorptivity is a property of the molecule that is absorbing the infrared radiation of a given wavelength and not of concentration. The more effective a molecule is in absorbing the infrared radiation of characteristic frequencies, the greater will be the extent of absorption (39).

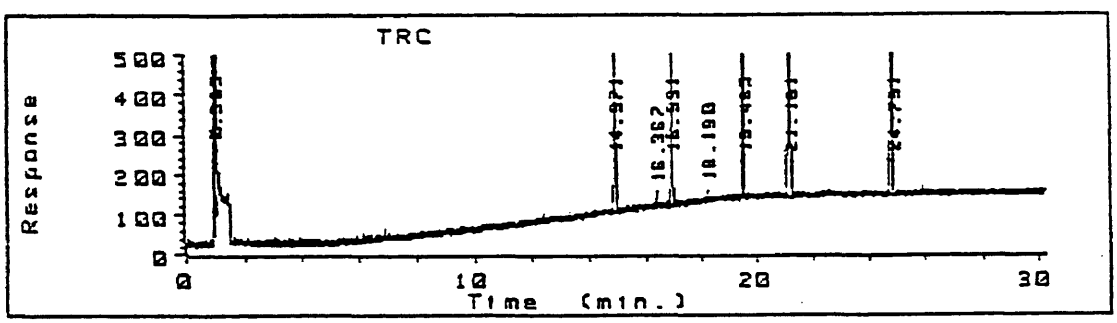

Figure 3. The total response chromatograph of the infrared detector for the freon soluble residue extracted from Tape A.

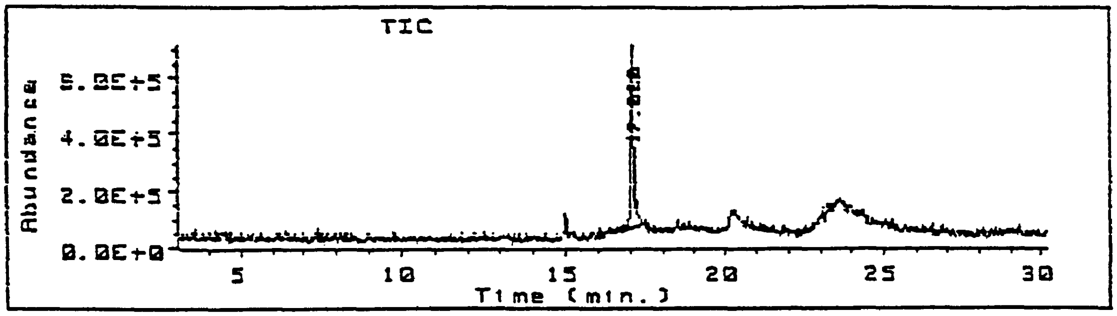

Figure 4. The total ion chromatograph of the mass spectrometry detector for the freon soluble residue extracted from Tape A.

At an evolution time of 14.9 minutes, an organic acid was detected by FTIR spectroscopy, and at an evolution time of 15.1 minutes, a compound with a molecular weight of 228 AMU was detected by MS. This information indicated that this compound was tetradecanoic acid ($CH_3(CH_2)_{12}COOH$). Although a smaller peak was observed by the FTIR detector at 16.4 minutes, no corresponding peak was clearly distinguishable in the TIC. The compound associated with this peak was also an organic acid of longer chain length than tetradecanoic acid. Selective ion mass spectrometry (SIMS) for a molecular weight of 256 AMU indicated that the organic acid was hexadecanoic acid ($CH_3(CH_2)_{14}COOH$).

Three compounds were detected by the FTIR detector at evolution times of 16.9, 19.5 and 21.2 minutes, and three compounds were detected by the MS detector at evolution times of 17.1, 20.2 and 23.6 minutes. The FTIR and MS results suggest that these three compounds were fatty acid esters similar to butoxy ethyl stearate ($C_{17}H_{35}COOC_2H_4OC_4H_9$) or a tetradecanoic acid ester. Exact identification of these fatty acid esters is difficult because FTIR spectroscopy does not detect chain lengths and no dominant molecular ions were detected by MS for the ester functional groups, which are ionized during the vaporization process.

Finally, a difunctional ester was detected by FTIR spectroscopy at an evolution time of 24.8 minutes, but no corresponding compound was detected by MS. Reasons for not detecting the difunctional ester by MS may be poor resolution and loss of sensitivity due to limited volatility of this component.

The TRC of the Freon soluble residue extracted from Tape B is shown in Figure 5 and the TIC in Figure 6. The TRC shows two major peaks at 16.4 and 17.7 minutes, and two broad regions with peaks ranging from 23 to 26 minutes and from 27 to 31 minutes. The TIC for Tape B has one distinct peak at 16.6 minutes and a broad peak in the range of 25 to 40 minutes.

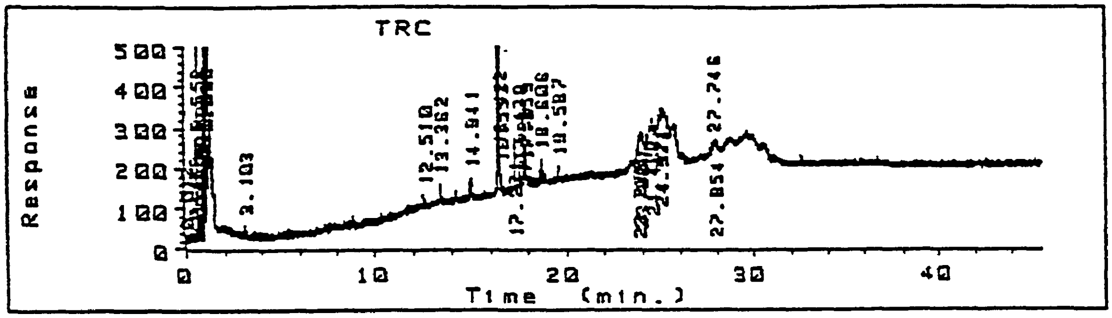

Figure 5. The total response chromatograph of the infrared detector for the freon soluble residue extracted from Tape B.

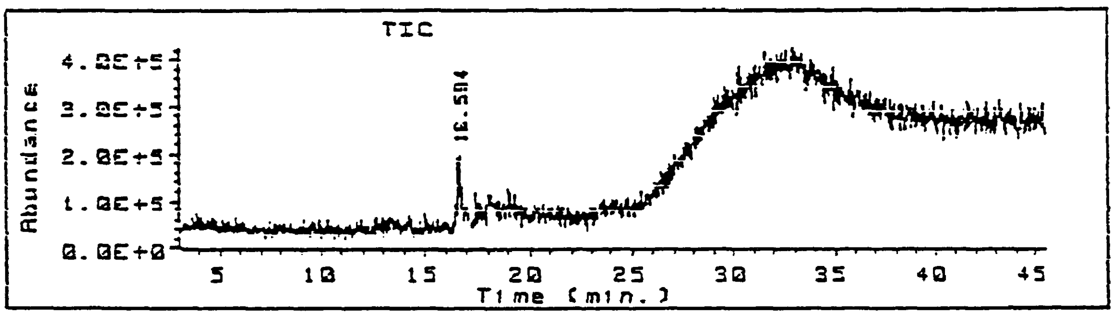

Figure 6. The total ion chromatograph of the mass spectrometry detector for the freon soluble residue extracted from Tape B.

At an evolution time of 16.4 minutes, an organic acid was detected by FTIR spectroscopy, and at an evolution time of 16.6 minutes, a compound with a molecular weight of 256 AMU was detected by MS. This information indicated that this first detected component was hexadecanoic acid. At an evolution time of 17.7 minutes a second organic acid with a longer chain length was detected by FTIR spectroscopy, but was not clearly distinguishable in the TIC. The use of SIMS for a molecular weight of 284 AMU confirmed that the organic acid was octadecanoic acid ($CH_3(CH_2)_{16}COOH$).

A smaller peak was observed by the FTIR detector at 14.9 minutes, but again no corresponding peak was clearly distinguishable in the TIC. The compound associated with this peak was also an organic acid of shorter chain length than hexadecanoic acid. Using SIMS for a molecular weight of 228 AMU confirmed that this fatty acid was tetradecanoic acid. Notice in Figure 5 a small peak also existed at an evolution times of 13.4 minutes. Using SIMS for a molecular weight of 200 AMU indicated that this compound was dodecanoic acid ($CH_3(CH_2)_{10}COOH$), a fatty acid with an even smaller chain length than tetradecanoic acid.

As previously mentioned, the TRC for the extracted residue from Tape B (Figure 5) has two broad regions with peaks ranging from 23 to 26 minutes and from 27 to 31 minutes, and the TIC (Figure 6) has a broad peak in the range of 25 to 40 minutes. The FTIR and MS detectors indicated that these regions were associated with a variety of esters of hexadecanoic acid. Some of the peaks in these regions may be isomers of the same compound.

The TRC of the extracted residue from Tape C is shown in Figure 7 and the TIC in Figure 8. The TRC shows one distinct peak at 16.4 minutes and two broad regions with peaks from 23 to 26 minutes and from 27 to 31 minutes. The TIC for Tape C only shows a broad peak in the range of 25 to 40 minutes.

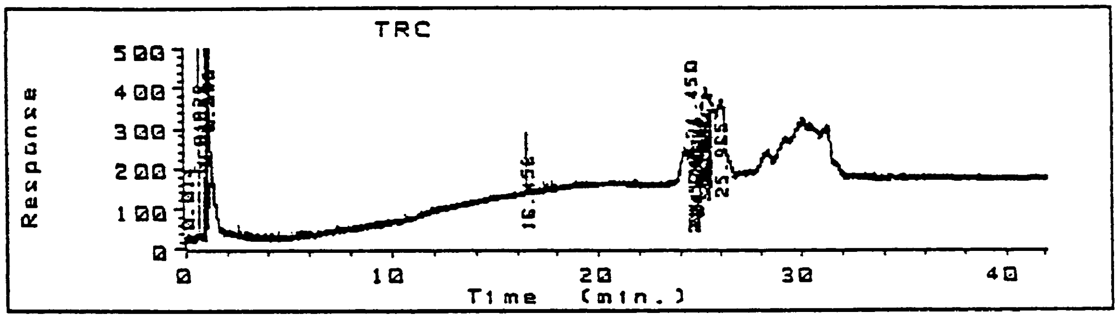

Figure 7. The total response chromatograph of the infrared detector for the freon soluble residue extracted from Tape C.

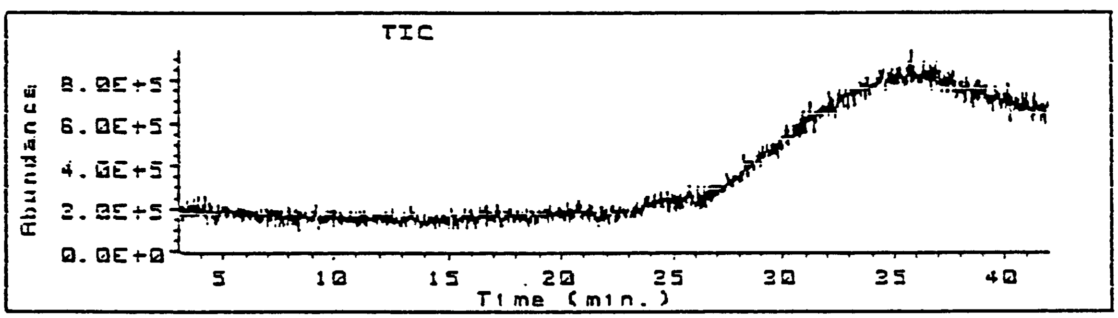

Figure 8. The total ion chromatograph of the mass spectrometry detector for the freon soluble residue extracted from Tape C.

At an evolution time of 16.4 minutes, an organic acid was detected by FTIR spectroscopy, but not clearly distinguishable in the TIC. The FTIR detector evolution time was the same as that for hexadecanoic acid, which was identified in the extracted residue from Tape B. The use of SIMS for a molecular weight of 256 AMU confirmed that the organic acid was hexadecanoic acid.

The TRC for the extracted residue from Tape C (Figure 7) also has two broad regions with peaks, from 23 to 26 minutes and from 27 to 31 minutes, and the TIC (Figure 8) has a broad peak in the range of 25 to 40 minutes. As with the extracted residue from Tape B, the FTIR and MS detectors indicated that these regions were associated with a variety of esters of hexadecanoic acid.

The TRC of the extracted residue for Tape D is shown in Figure 9 and the TIC in Figure 10. The TRC shows three distinct peaks (at 14.9, 20.4, and 25.3 minutes) and two broad regions with peaks ranging from 24 to 26 minutes and from 27 to 31 minutes. The TIC for Tape B has one distinct peak at 15.2 minutes and a broad peak in the range of 26 to 35 minutes.

Tetradecanoic acid was detected by the FTIR detector at an evolution time of 14.9 minutes and by the MS detector at 15.2 minutes. The FTIR detector identified the two peaks at 20.4 and 25.3 minutes as difunctional esters, such as dibutyl ester of 1,8-octanedicarboxylic acid. The presence of two peaks suggests that there were two esters with different molecular weights. These compounds were not detected by the MS detector.

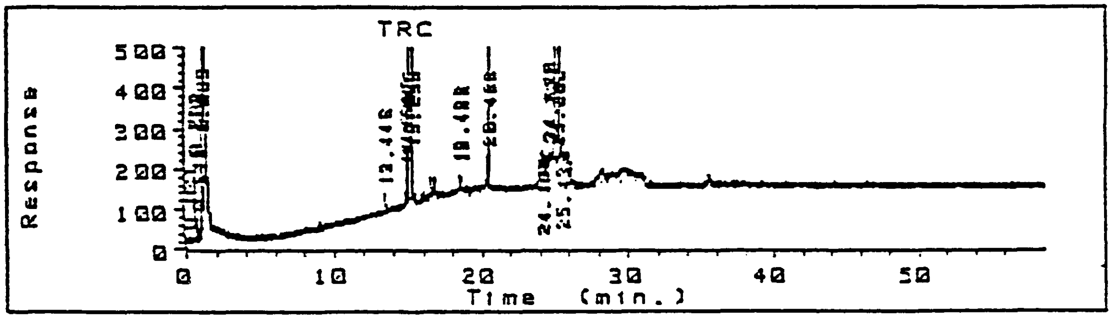

Figure 9. The total response chromatograph of the infrared detector for the freon soluble residue extracted from Tape D.

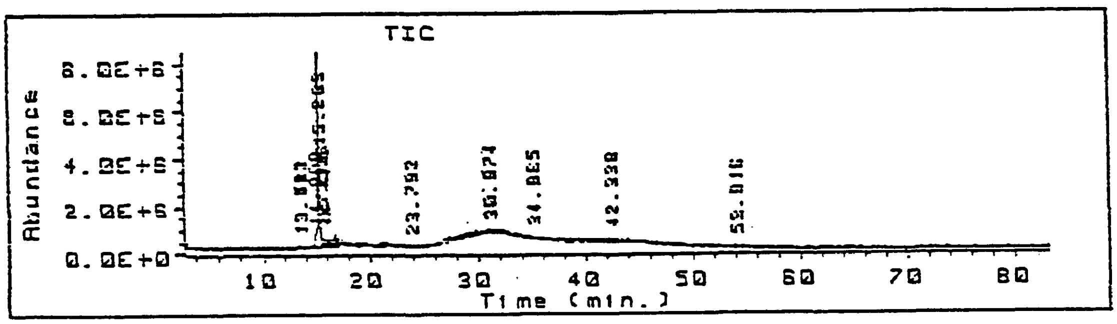

Figure 10. The total ion chromatograph of the mass spectrometry detector for the freon soluble residue extracted from Tape D.

The TRC for the extracted residue from Tape D (Figure 9) also has two broad regions with peaks, from 24 to 26 minutes and from 27 to 31 minutes, and the TIC (Figure 10 has a broad peak in the range of 26 to 35 minutes. As with the extracted residues from Tapes B and C, the FTIR and MS detectors indicated that these regions were associated with a variety of esters of hexadecanoic acid.

A summary of the freon soluble components for the four tapes is presented in Table 3. All of these components are known to have been used as lubricants in magnetic tape (4,5,6).

Table 3

Summary of Freon Soluble Residues

Tape	Components
A	Tetradecanoic Acid Hexadecanoic Acid Fatty Acid Esters Difunctional Esters
B	Dodecanoic Acid Tetradecanoic Acid Hexadecanoic Acid Octadecanoic Acid Fatty Acid Esters
C	Hexadecanoic Acid Fatty Acid Esters
D	Tetradecanoic Acid Fatty Acid Esters Difunctional Esters

3.1.2 FTIR Analysis of Acetone Soluble Residues.

FTIR analysis was used to identify the residues extracted from each tape with acetone. The FTIR spectra for the acetone soluble residues for tapes A through D are shown in Figures 11 through 14. For comparison a spectrum of a polyester-polyurethane is shown in Figure 15. The similarities indicate that the acetone soluble residues extracted from all four tape samples are polyester-polyurethane materials. Polyester-polyurethanes were noted in section 1.3 to be commonly used as binders in magnetic tape. Notice in Figures 11 through 14 that no excess isocyanate groups (R-N=C=O) were detected in the wavenumber range of 2250 to 2300 cm^{-1}. Since isocyanates are used as the active component in the polyurethane systems, the FTIR results indicate that the isocyanates were fully reacted.

In Figure 11, there is a small peak at a wavenumber of 2350 cm^{-1}. This peak occurred in the region for carbon dioxide. The presence of this peak indicated that there was more carbon dioxide at the surface of the residue sample than at the surface of the blank test cell. Recall from section 2.1.4 in the procedures that the blank spectrum of the test cell was electronically subtracted from the sample spectrum. In Figures 12 through 14, there is a negative peak at the same wavenumber. These negative peaks were caused by the presence of more carbon dioxide at the surface of the blank test cells than at the surface of the residue samples.

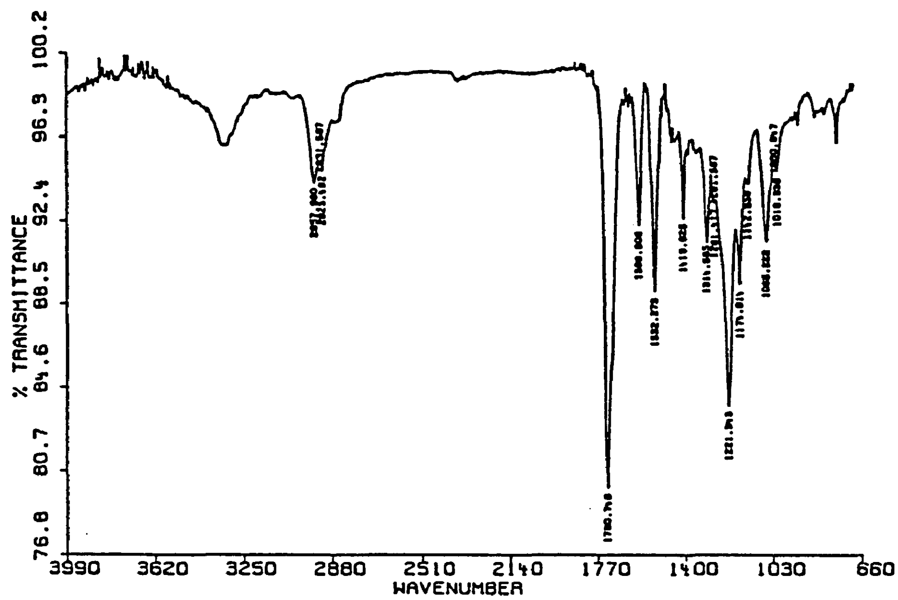

Figure 11. Spectrum of the acetone extracted residue for tape A. The spectrum indicates that the residue was a polyester-polyurethane.

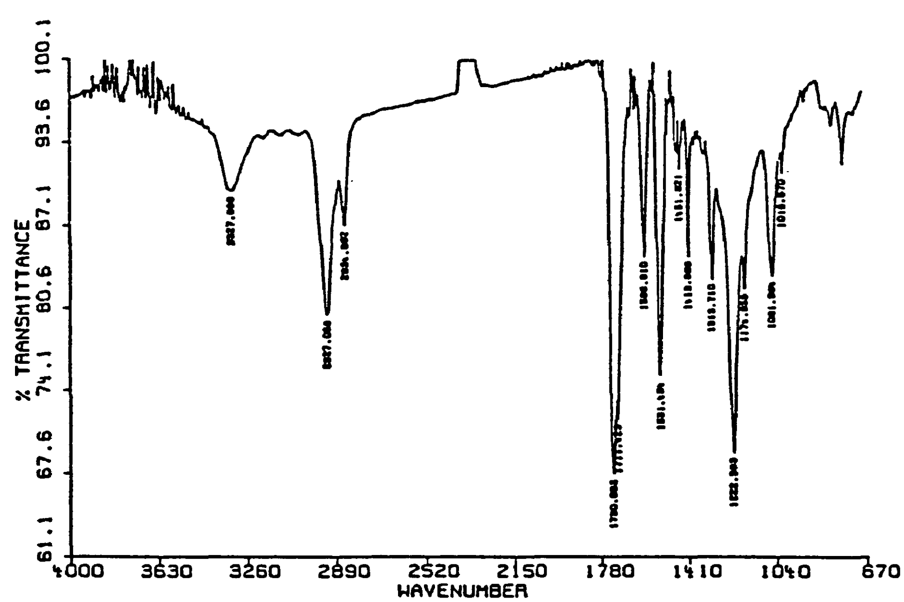

Figure 12. Spectrum of the acetone extracted residue for tape B. The spectrum indicates that the residue was a polyester-polyurethane.

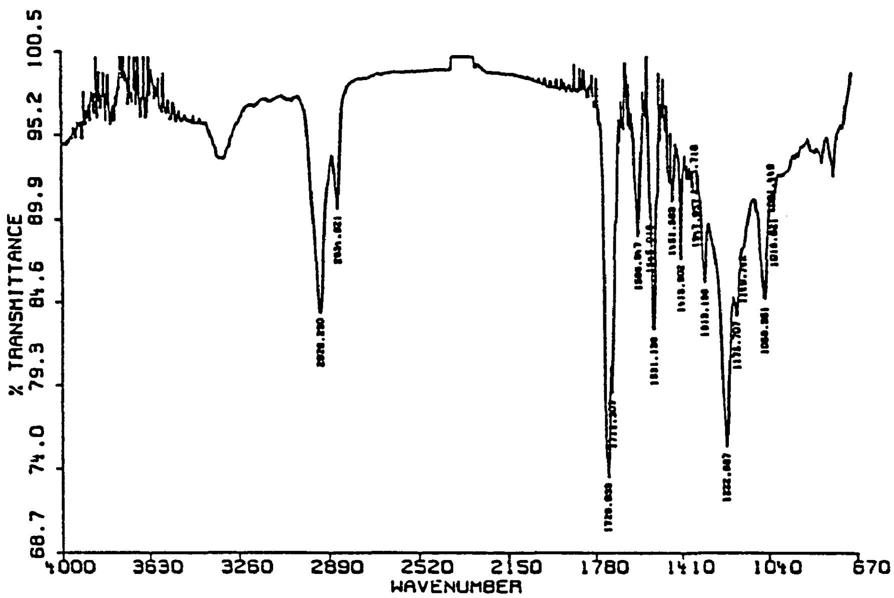

Figure 13. Spectrum of the acetone extracted residue for tape C. The spectrum indicates that the residue was a polyester-polyurethane.

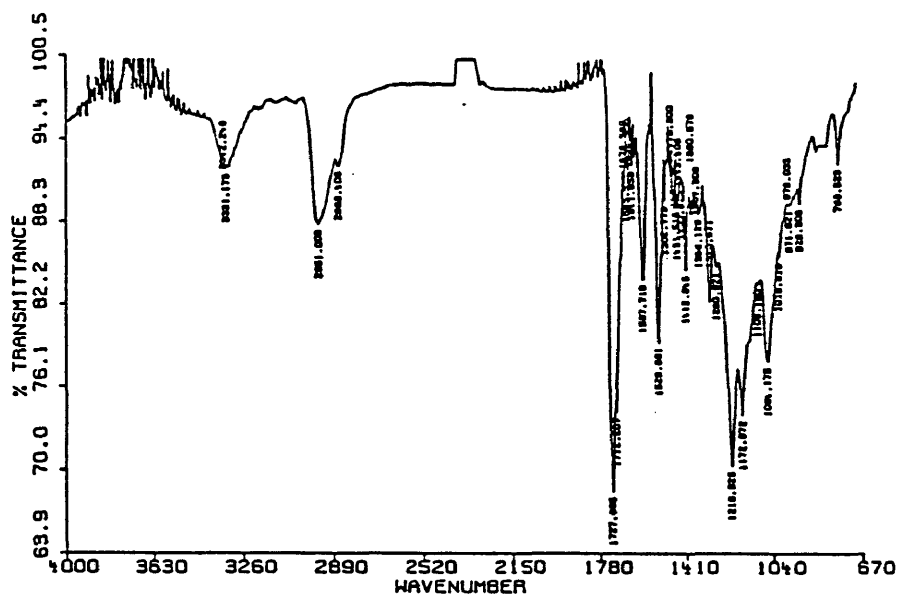

Figure 14. Spectrum of the acetone extracted residue for tape D. The spectrum indicates that the residue was a polyester-polyurethane.

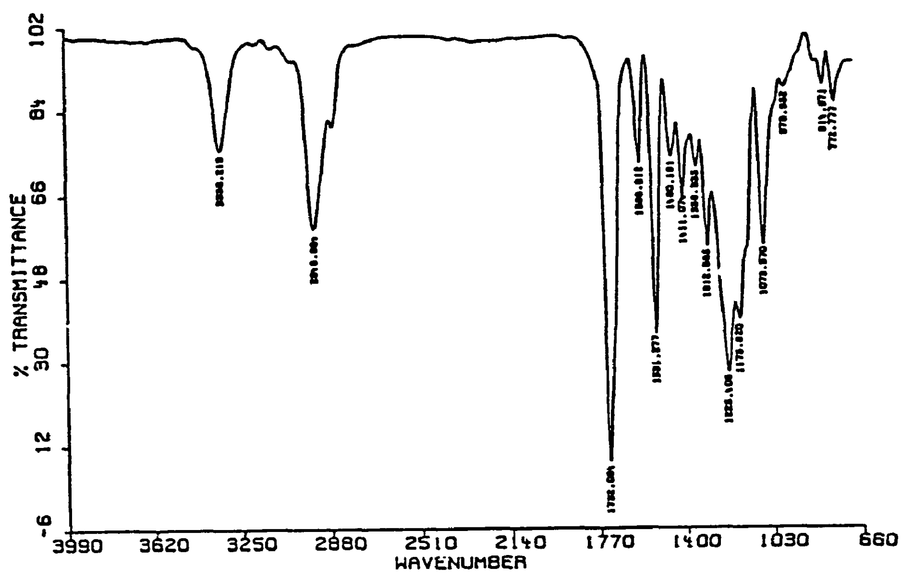

Figure 15. Spectrum of a polyester-polyurethane. Copyright 1986 Nicolet Instrument Corporation, reprinted with permission.

3.1.3 <u>FTIR Analysis of Base Film Materials</u>.

FTIR was used to identify the base film material in each tape. The FTIR spectra of the base film materials for tapes A through D are shown in Figures 16 through 19. For comparison, a spectrum of polyethylene terephthalate is shown in Figure 20. The similarities indicate that the base film material for all four tape samples was PET.

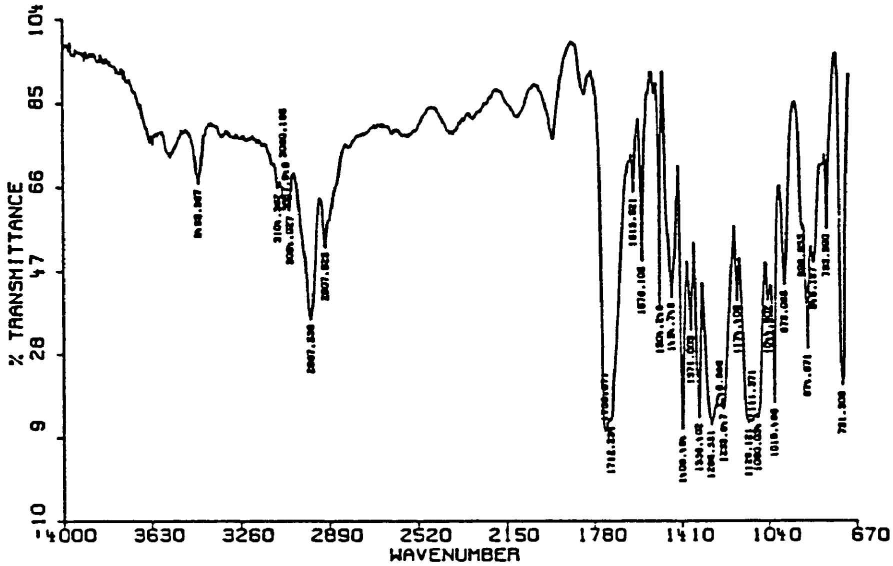

Figure 16. Spectrum of the base film material for tape A. The spectrum indicates that the film material was PET.

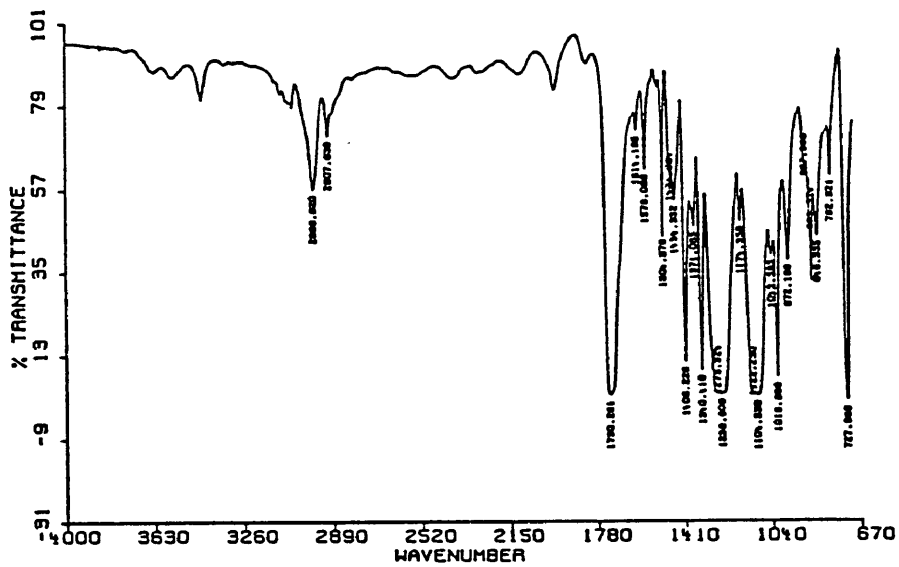

Figure 17. Spectrum of the base film material for tape B. The spectrum indicates that the film material was PET.

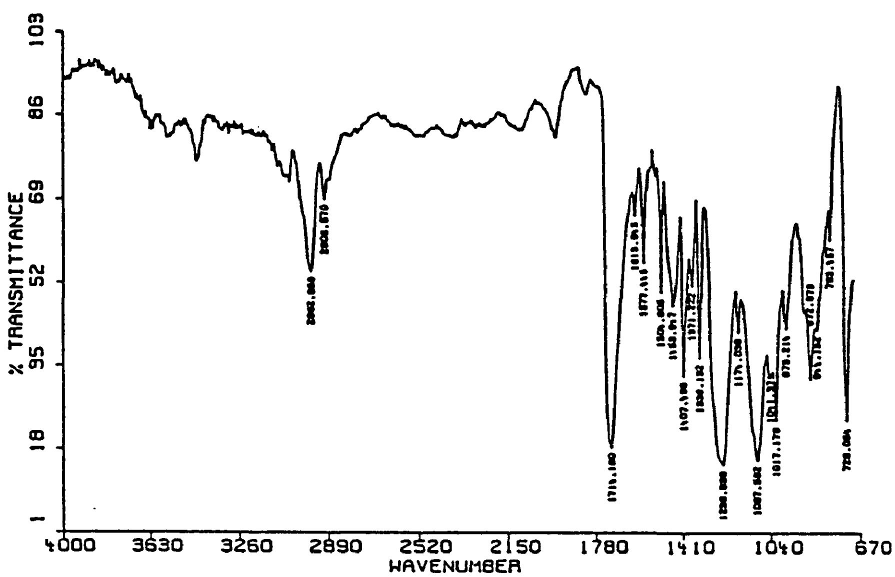

Figure 18. Spectrum of the base film material for tape C. The spectrum indicates that the film material was PET.

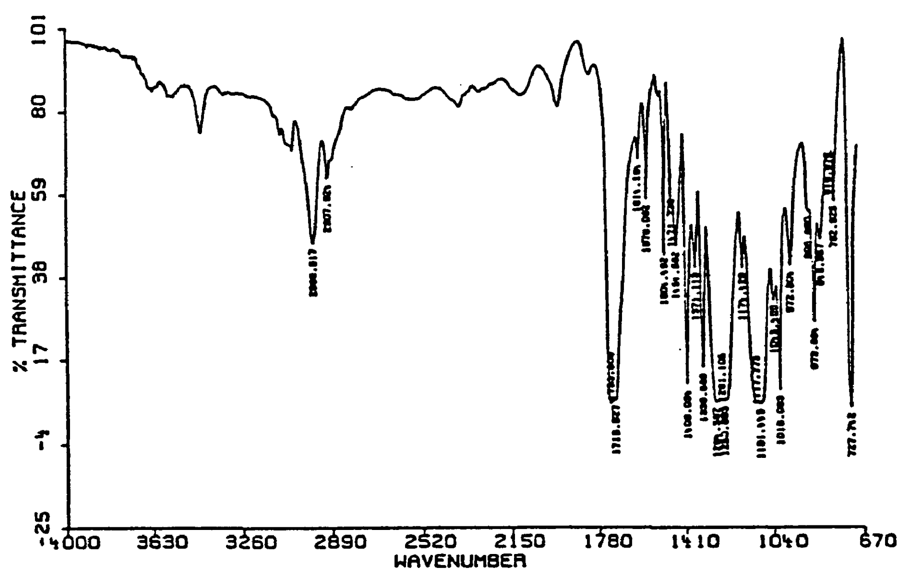

Figure 19. Spectrum of the base film material for tape D. The spectrum indicates that the film material was PET.

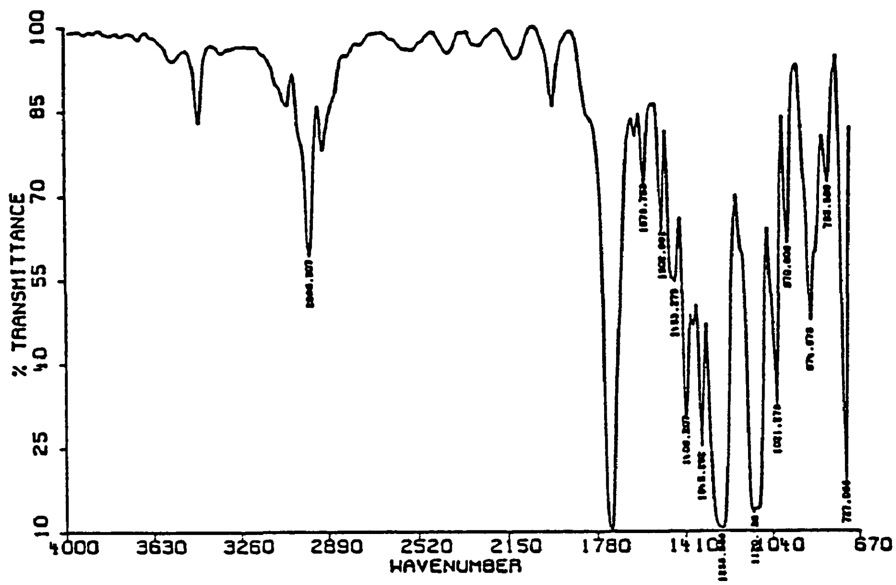

Figure 20. Spectrum of a polyethylene terephthalate. Copyright 1986 Nicolet Instrument Corporation, reprinted with permission.

3.1.4 ESCA Analysis of Magnetic Coatings.

ESCA was used to provide chemical state information about the surfaces of each magnetic tape, in particular about the magnetic particles. Figures 21 through 24 are the survey spectra taken of Tapes A through D. These spectra indicate that chromium, oxygen, carbon and nitrogen were present on the surface of all four tapes.

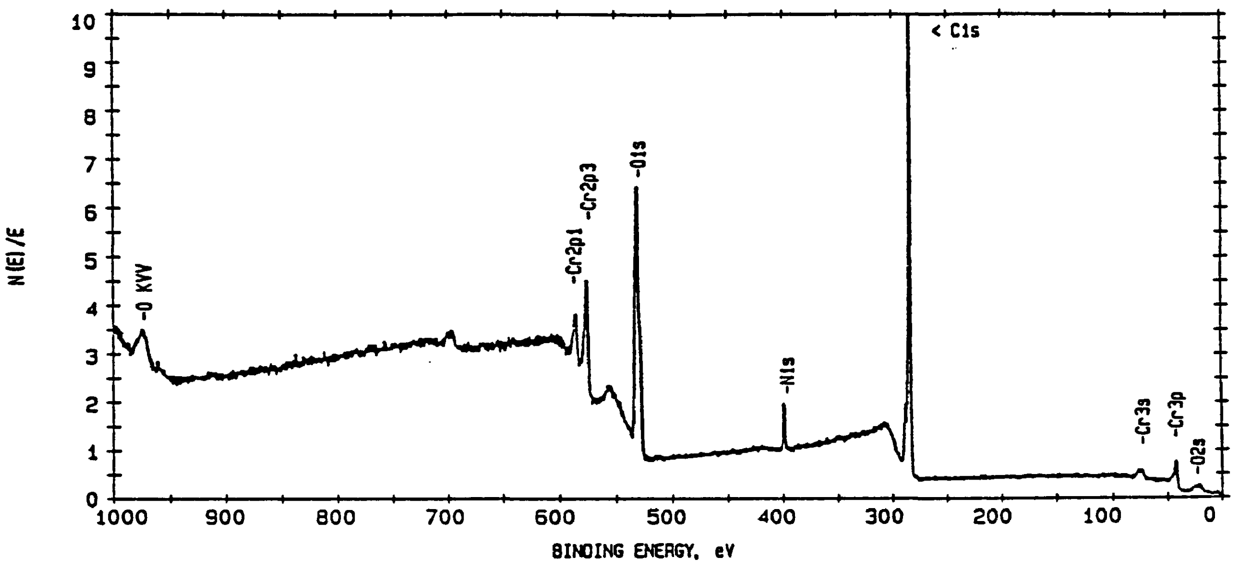

Figure 21. ESCA survey spectrum of the surface of Tape A.

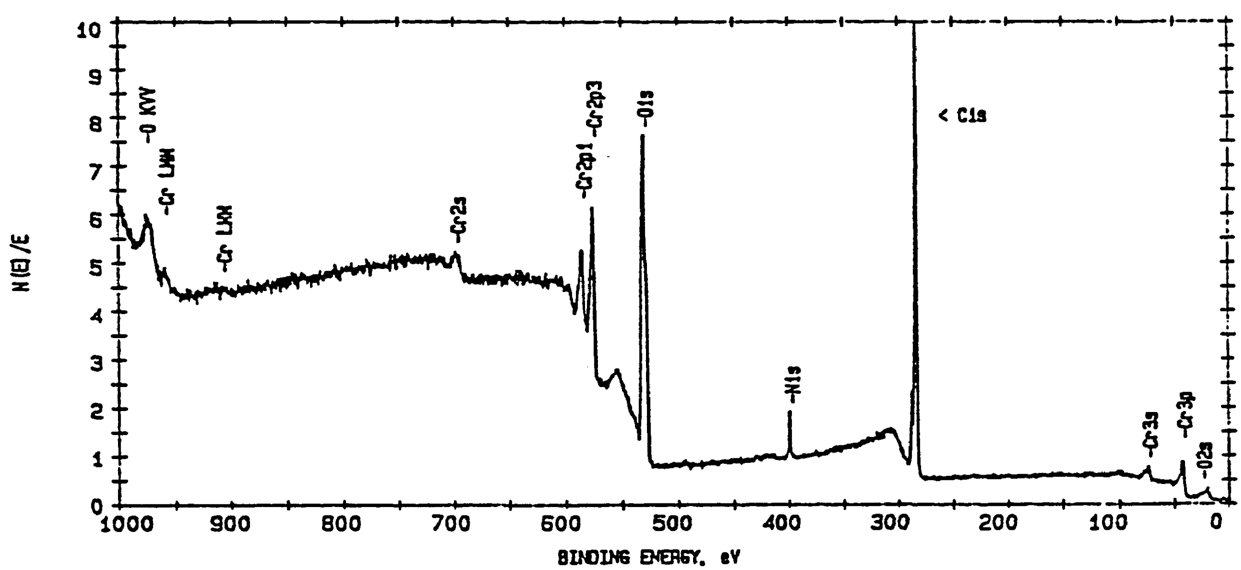

Figure 22. ESCA survey spectrum of the surface of Tape B.

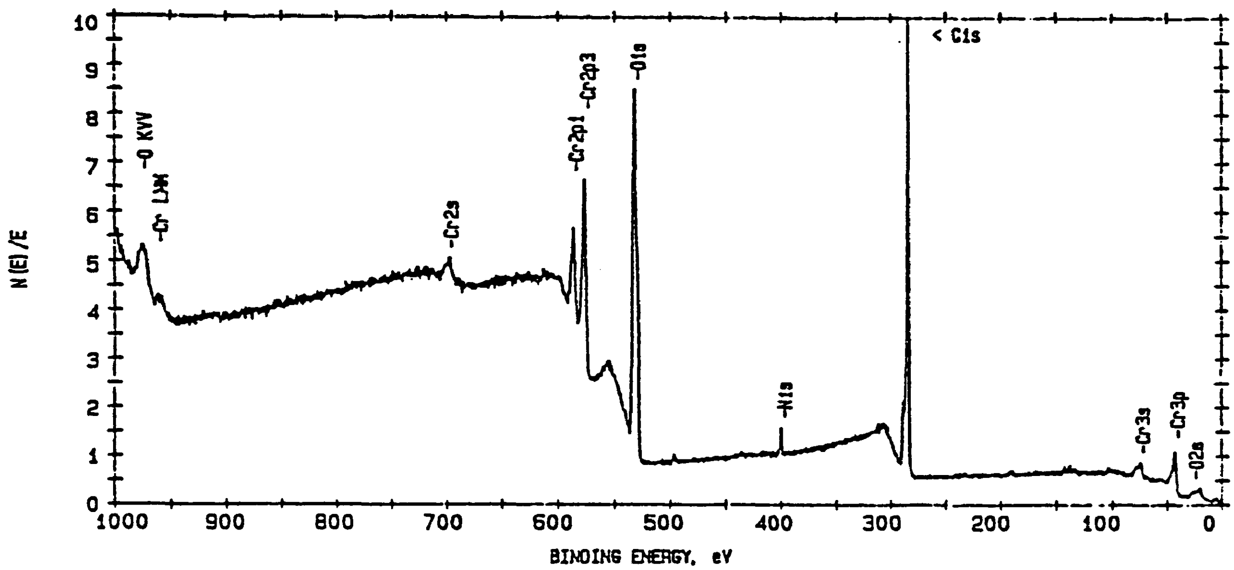

Figure 23. ESCA survey spectrum of the surface of Tape C.

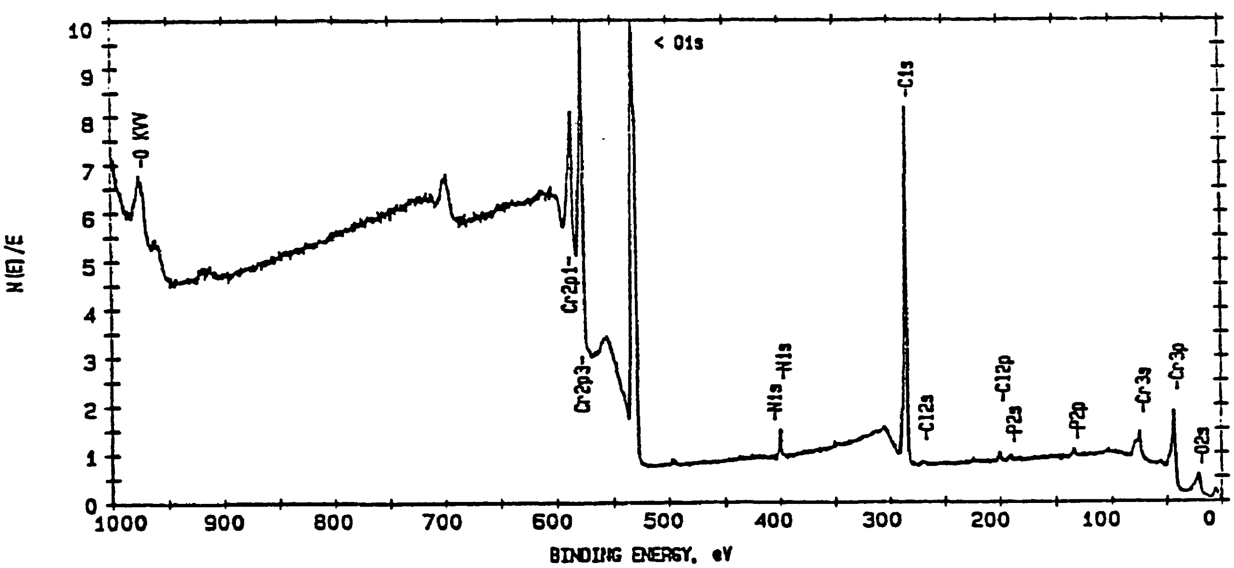

Figure 24. ESCA survey spectrum of the surface of Tape D.

The peaks at approximately 576 and 586 eV in each survey spectrum (Figures 21 to 24) are associated with the chromium $2p_{3/2}$ and $2p_{1/2}$ electrons respectively. Multiplet splitting of the 2p chromium electrons occurs because of its unpaired electrons in the valence levels. It is caused by coupling of electron spins in the ion produced by photoionization, resulting in two different final states (33).

The chromium region of the survey spectrum for Tape A is shown in Figure 25. This region of the spectrum was similar for all four tapes. Chromium photoelectrons at these energies are associated with chromium dioxide (32, 33). Notice, however, that the relative heights of the chromium peaks in the survey spectra for tapes A, B and C (Figures 21 through 23) are similar, but are noticeably higher for Tape D (Figure 24). This suggests that the relative quantity of chromium dioxide at the surface of tape D is greater than that at the surface of tapes A, B and C.

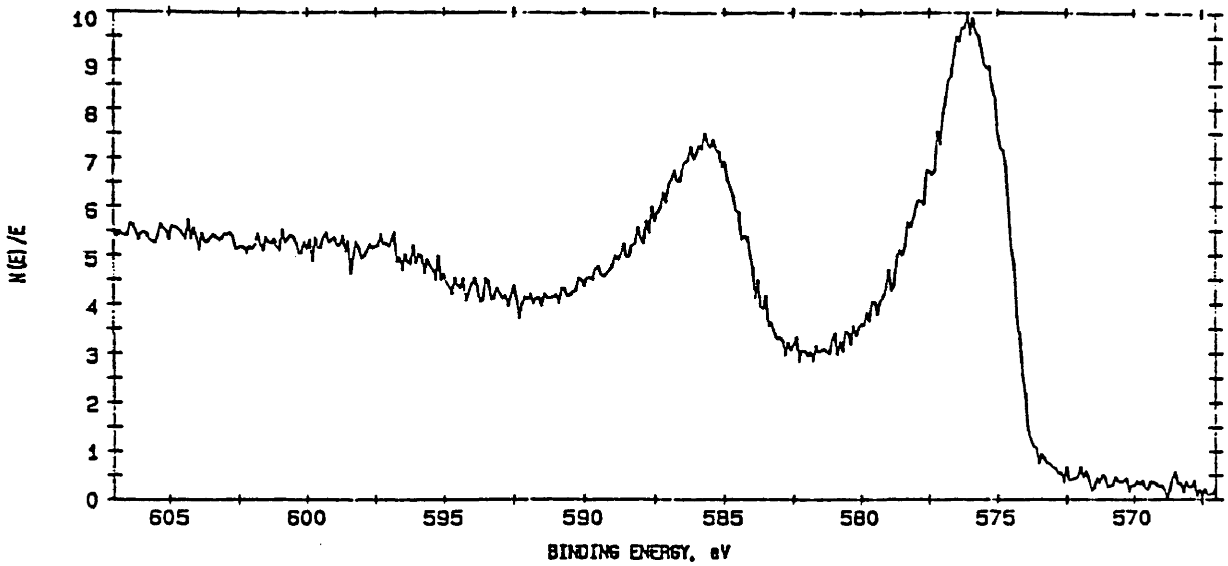

Figure 25. The chromium region of the ESCA survey spectrum for Tape A. This region was similar for Tapes A, B, C and D.

The peak at approximately 532 eV in all four survey spectra (Figures 21 to 24) is associated with the oxygen 1s electron. The oxygen region of the survey spectrum for Tape A is shown in Figure 26. This region of the spectrum was similar for Tapes A, B and C. The oxygen region of the survey spectrum for Tape D is shown in Figure 27. Oxygen photoelectrons at an energy of 528.3 eV are associated with oxides (32,33). Notice the difference in the relative peak height at this energy in Figures 26 and 27. The greater peak height for Tape D is consistent with the finding that the relative quantity of chromium dioxide at the surface of tape D was greater than that at the surface of tapes A, B and C. Other oxygen peaks can be associated with a variety of hydrogen-oxygen, carbon-oxygen, and hydrogen-carbon-oxygen bonds, both single and multiple. These types of chemical states were expected because both the lubricant and binder in the tape contain these types of bonds.

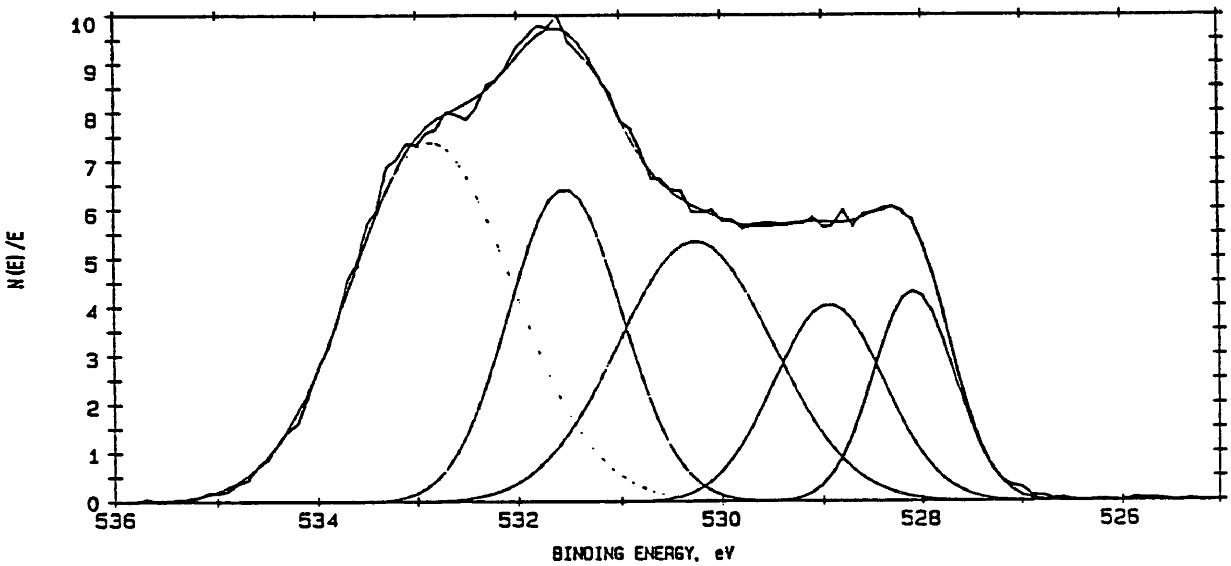

Figure 26. The oxygen region of the ESCA survey spectrum for Tape A. This region was similar for Tapes A, B and C.

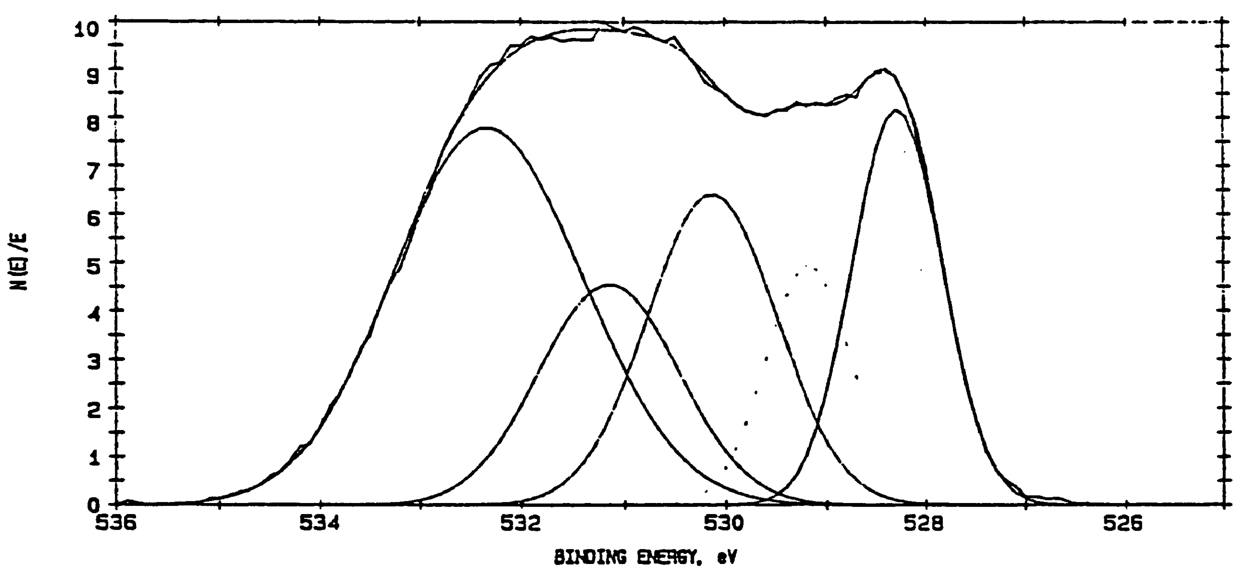

Figure 27. The oxygen region of the ESCA survey spectrum for Tape D.

The peak at approximately 285 eV in all four survey spectra (Figures 21 to 24) is associated with the carbon 1s electron. Figure 28 shows the carbon region of the survey spectrum for Tape A. This region of the spectrum was similar for all four tapes. The carbon photoelectrons at an energy of approximately 285 eV are associated with carbon-carbon and carbon-hydrogen bonds (32, 33). The carbon photoelectrons at an energy of approximately 289 eV are associated with carbon-oxygen bonds (32, 33). These types of chemical states were expected because both the lubricant and binder in the tape contain these types of bonds.

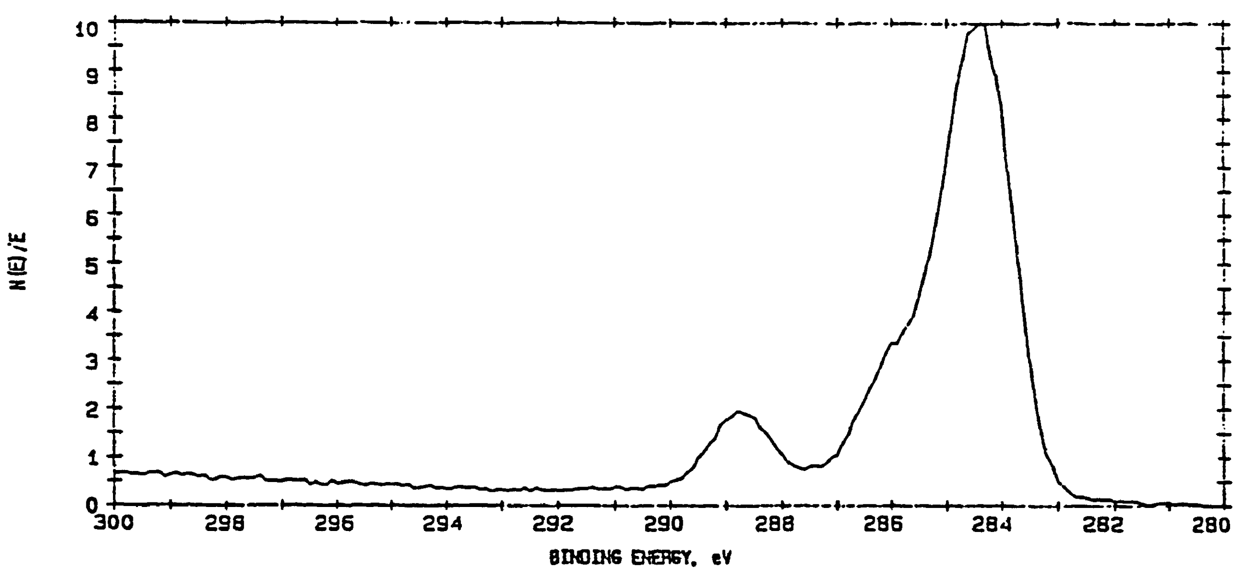

Figure 28. The carbon region of the ESCA survey spectrum for Tape A.

The peak at approximately 398 eV in all four survey spectra (Figure 21 to 24) is associated with the nitrogen 1s electron. Nitrogen was expected to be found in the survey spectra of each tape, because nitrogen is also a constituent of the polyurethane elastomer binder.

3.1.5 SEM Analysis of Magnetic Coating.

The SEM was used to document the morphology of the surface features of the magnetic particles. Figure 29 shows a relatively low magnification (1000x) photomicrograph of the surface features of Tape B using a spot size of 100 nanometers. The features of this photomicrograph show a highly packed and highly oriented magnetic particle density. The dark spots in the photomicrograph are regions depleted of magnetic particles. Binder is most likely to reside in these regions. Definition of the binder did not appear on the photomicrograph because the electrons generated by the 25 kilovolt electron beam were absorbed by the binder.

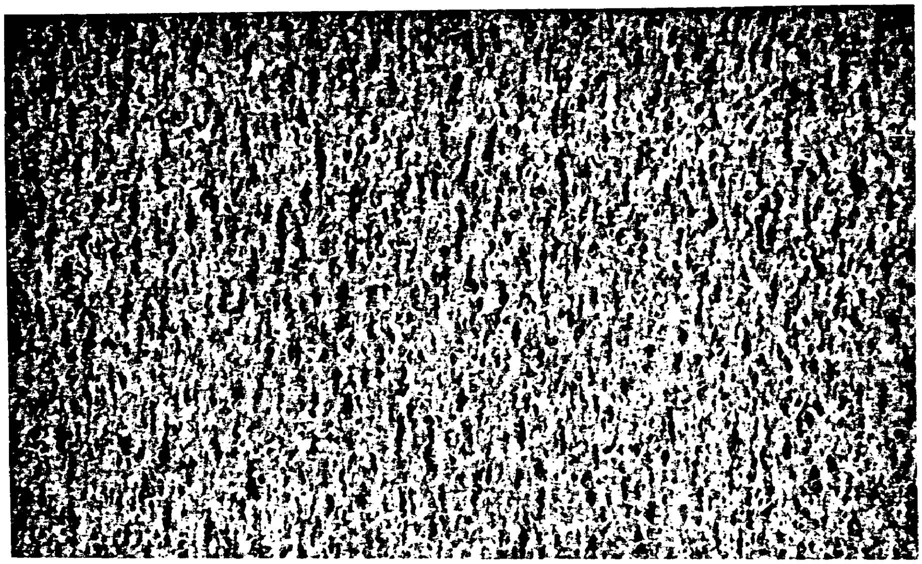

Figure 29. SEM photomicrograph of the surface features for Tape B (1000x).

Figure 30 shows a relatively high magnification (10,000x) photomicrograph of the surface features of Tape B using a spot size of 20 nanometers. This photomicrograph shows that the orientation of the individual magnetic particles are relatively acicular in shape. It is difficult to resolve exact particle size from this photomicrograph because the particles were embedded in the magnetic coating in a variety of orientations. To determine particle sizes, the binder would have to be removed by a technique such as plasma etching.

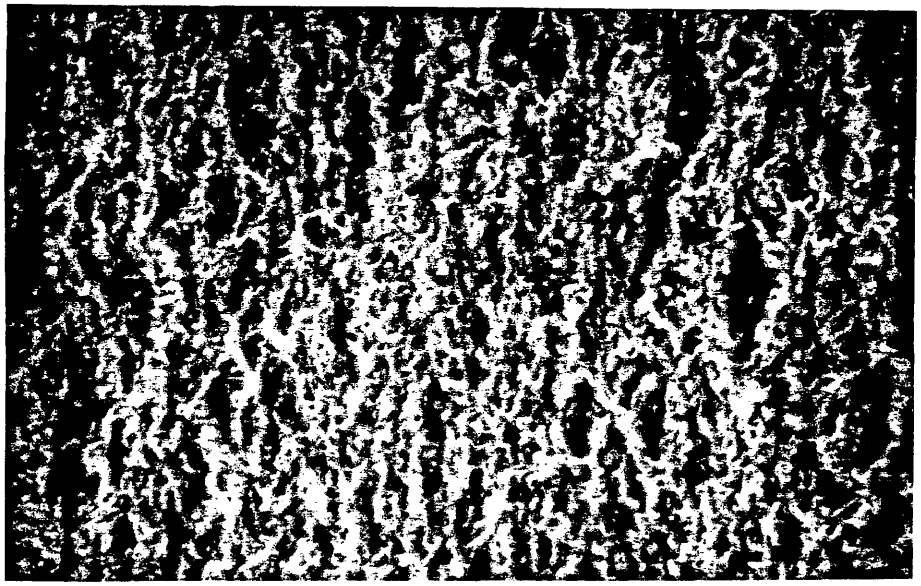

Figure 30. SEM photomicrograph of the surface features for Tape B (10,000x).

Figure 31 shows a spectrum of the magnetic particles using energy dispersive spectroscopy (EDS). The chemistry of the magnetic particles were identified as chromium-oxygen rich particles. The chromium (Cr) fingerprint occurs as a double peak at 5.4 and 5.9 eV. The oxygen (O) fingerprint occurs at 0.53 eV. The peaks identified in Figure 31 coincide with these fingerprints. These results agree with the ESCA results in the previous section for the magnetic coating chemistry.

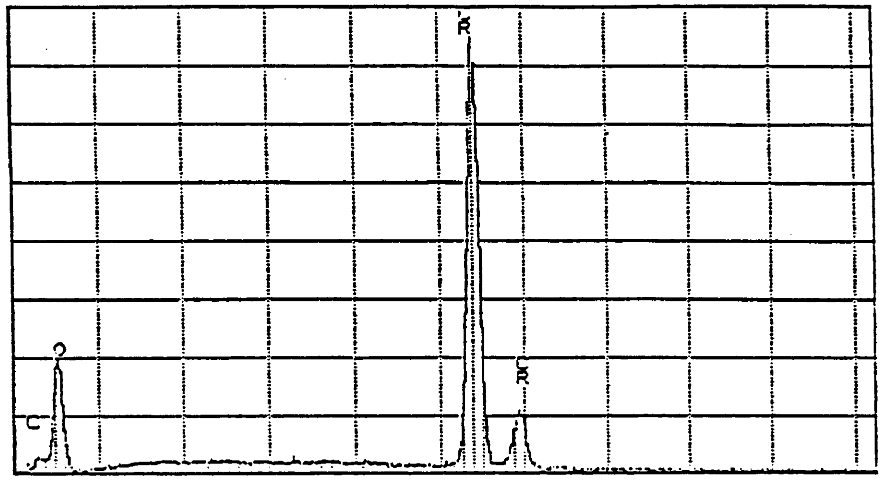

Figure 31. EDS spectrum of the magnetic particles from Tape B indicating chromium-oxygen rich particles.

3.1.6 Gravimetric Analysis of Base Films.

Gravimetric analysis was used to determine the amount of base film in each tape relative to the whole tape. Table 4 presents the weight percent of the base film materials after stripping the magnetic coating. The data in this table is based on three samples and shows that the average weight percent of the base film material ranges from 76.6% for Tape D to 80.4% for Tape A. One reason for the lower average weight percent for Tape D is that the base film for this tape was coated with binder and magnetic particles on both sides. Assuming that the volume of the base film from each tape was similar, the additional back-coating on Tape D reduced the relative percentage of the base film.

Table 4

Gravimetric Analysis of Base Films

Tape	Base Film (%) Sample #1	Sample #2	Sample #3	Average
A	80.2%	80.0%	81.0%	80.4%
B	78.1%	78.4%	78.1%	78.2%
C	79.3%	80.2%	79.5%	79.7%
D	76.2%	76.6%	76.9%	76.6%

3.1.7 TGA of Base Films.

Thermogravimetric analysis (TGA) was performed on base film samples from each magnetic tape to provide information about the degradation of these materials. The rate determining step in the degradation of PET is believed to be random chain scission in the ester linkages (see structure on page 8). The methylene group is believed to be the main point of weakness (9,22,40). The thermogram of a base film sample from Tape A and its first derivative are shown in Figure 32. The thermograms and first derivatives for Tapes B, C and D were similar to those shown in Figure 32.

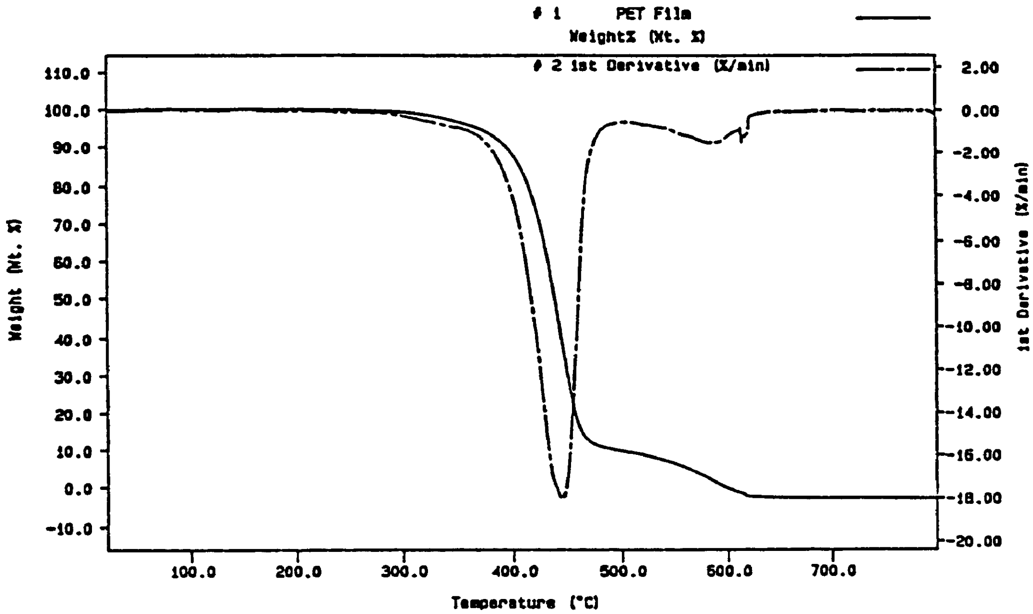

Figure 32. Thermogram of the base film material for Tape A.

The degradation onset temperatures of the base films are summarized in Table 5. The degradation onset temperature is defined as the intersection point of the extrapolated baseline before any weight loss occurs due to degradation with the tangent to the degradation curve. The tangent was taken at the inflection point in the degradation curve as identified by a peak in the first derivative of the original curve. The degradation onset temperatures ranged from 407°C for Tape A to 417°C for Tape C. These onset temperatures are dependent on the heating rate since the degradation of PET is a time-dependent process (40).

Table 5

TGA Degradation Onset Temperatures of Base Film Materials

Tape	Onset Temperature (°C)
A	407
B	416
C	417
D	415

3.1.8 TGA of Magnetic Tapes.

TGA was performed on samples from each magnetic tape to determine the weight percent of chromium dioxide in each tape. The thermogram of a sample from Tape A and its first derivative are shown in Figure 33. The thermograms and first derivatives for Tapes B, C and D were similar to those shown in Figure 33.

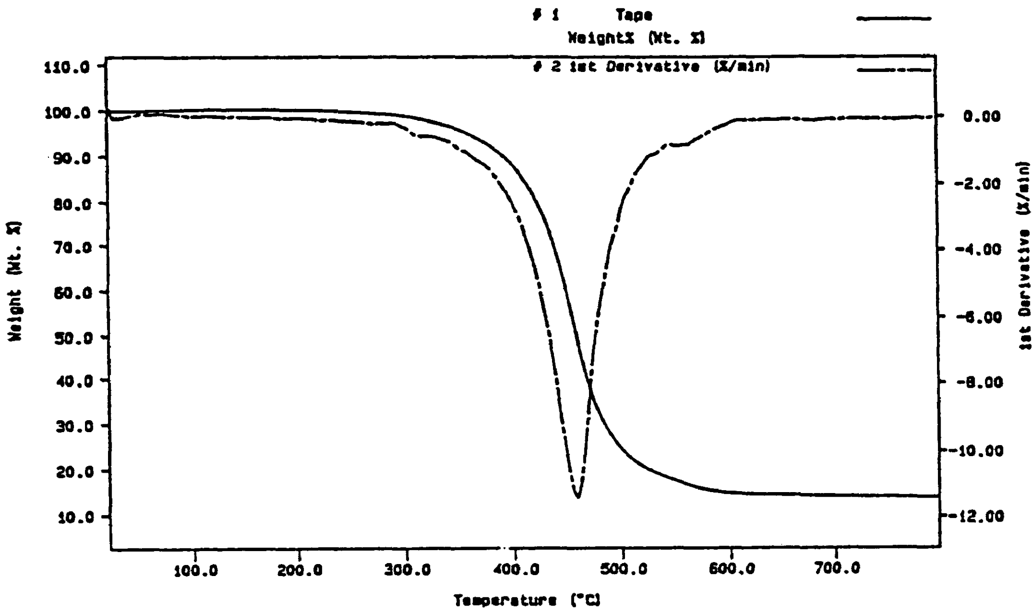

Figure 33. Thermogram and first derivative of Magnetic Tape A.

The onset of degradation for each tape is shown in Table 6. These results were similar to those for the base film listed in Table 5. The primary reason for the similarity was because of the high weight percent of base film relative to the whole tape. Also shown in Table 6 are the weight percentages of the noncombustible residue at 800°C for each magnetic tape. These results are an average of three samples. Assuming complete combustion of all polymeric materials at 800°C, the noncombustible residue originated from the chromium dioxide (CrO_2) in the tape.

Table 6

Combustible Versus Noncombustible Residue from Magnetic Tapes in Weight Percent

Tape	Onset Temperature (°C)	Noncombustible Residue	Combustible Residue
A	407	13.8%	86.2%
B	412	14.1%	85.9%
C	407	14.6%	85.4%
D	412	13.2%	86.8%

The weight percent of noncombustible residue listed in Table 6 needs to be corrected in order to determine the weight percent of chromium dioxide in the original samples. This is because chromium dioxide begins to lose oxygen at about 300°C (41). As CrO_2 loses oxygen, Cr_2O_3 forms.

$$4CrO_2 \rightarrow 2Cr_2O_3 + O_2$$

Based on stoichiometry, a correction factor of approximately 9.5% should be added to the weight of the noncombustible residue in Table 6 to account for the loss of oxygen from chromium dioxide. In order to examine the accuracy of this correction factor, a TGA experiment was performed on a sample of chromium dioxide, manufactured by

Dupont for use in magnetic tape. The resulting thermogram is shown in Figure 34. This thermogram shows an approximate weight loss of 10% between 20°C to 800°C. Assuming the presence of some moisture or absorbed gasses in the original CrO_2 sample, the theoretical and experimental results coincide.

A change in color confirmed that Cr_2O_3 was formed during the TGA experiment. At the beginning of the experiment, the chromium dioxide had a brownish-black appearance. At the end of the experiment, the color of the noncombustible residue was green, which is the color of Cr_2O_3.

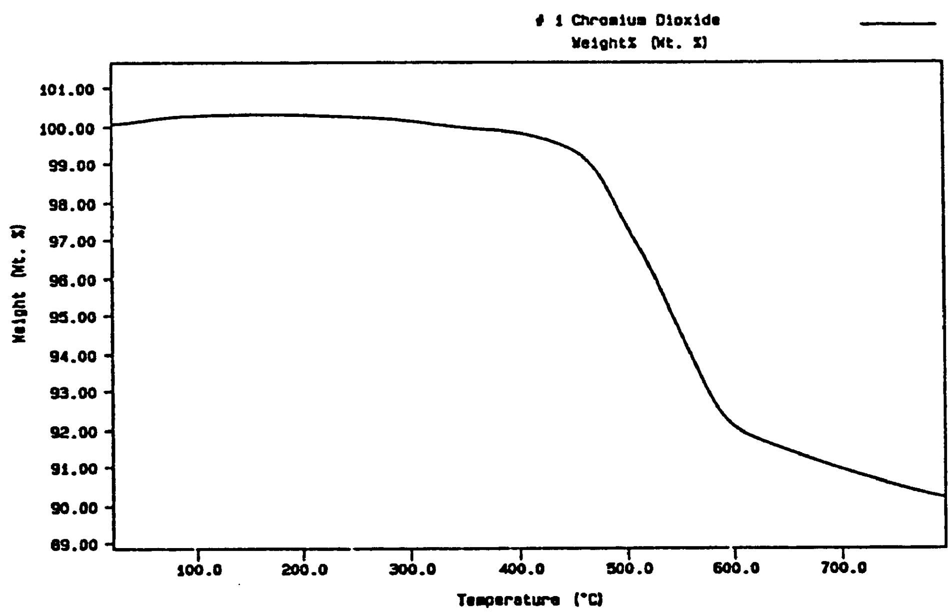

Figure 34. Thermogram for chromium dioxide. The thermogram indicates an approximate weight loss of 10%.

The relative quantities of the major components in each tape can now be estimated based on the gravimetric results for the base films in section 3.1.6 and on the correction for the noncombustible residue in Table 6. These results are summarized in Table 7. Notice that Tape D, which was coated on both sides, had the lowest percentage of chromium dioxide and base film.

Table 7

Relative Quantity of Components in Magnetic Tape

Tape	Base Film	Chromium Dioxide	Other Components*
A	80.4%	15.1%	4.5%
B	78.1%	15.4%	6.5%
C	79.5%	16.0%	4.5%
D	76.9%	14.5%	8.6%

* - This includes the lubricants, binder, and other volatile components.

3.2 Results of Transition Temperature Analysis

Three thermal analysis techniques were used to detect transition temperatures associated with the base film and binder. Those techniques were: differential scanning calorimetry (DSC), thermomechanical analysis (TMA) and dynamic mechanical analysis (DMA).

3.2.1 DSC Analysis of Base Films, Magnetic Tapes and Magnetic Coatings

Differential scanning calorimetry (DSC) was utilized to identify transitions of the polymeric components in the magnetic tape. First, base film samples from each tape were analyzed to isolate those transitions associated with the base film. Next, samples of magnetic tape were analyzed. Any detected transitions in the magnetic tape samples not associated with the base film could then be attributed to the binder. Finally, coating samples scraped from each tape were also analyzed as an alternate method to detect transitions associated with the binder.

Figure 35 shows the DSC curve for the PET base film from Tape B. The DSC curves for the base films from all four tapes were similar. Notice that only one event, an endothermic peak, was observed on this curve. This peak represents the melting of the crystalline portion of the PET base film.

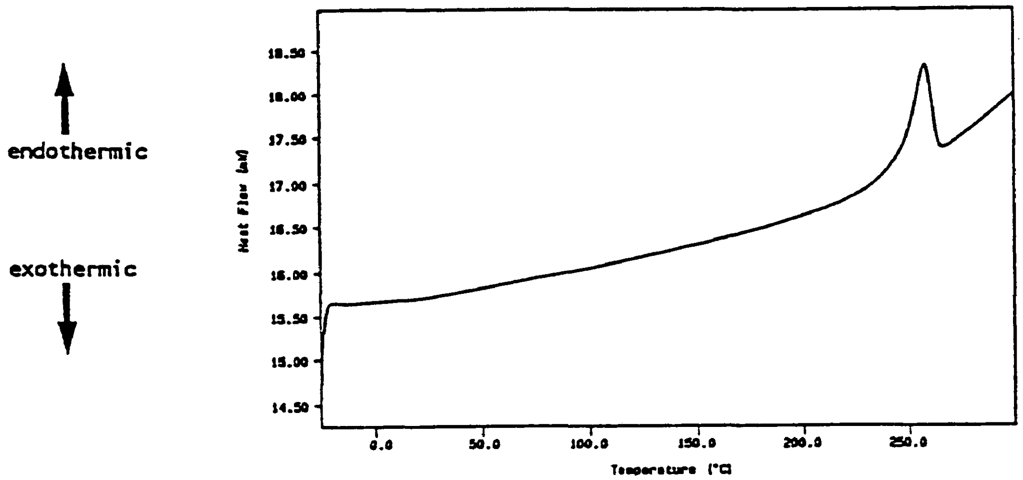

Figure 35. DSC curve for PET base film from Tape B. Only one melting transition was detected.

The results for all four base film materials are summarized in Table 8. As mentioned in section 1.7, polymers typically have a melting range because a sample consists of various molecular weights and crystal sizes. Therefore, Table 8 not only includes the melting peak temperature (T_{mp}) for each sample, but also each melting range identified by an initial temperature (T_{mi}) and a final temperature (T_{mf}). The melting peak temperatures ranged from 252.5°C for Tape C to 258.4°C for Tape B.

Table 8

DSC Results for Base Film Samples

Tape	T_{mp} (°C)	T_{mi} (°C)	T_{mf} (°C)	ΔH_f (J/g)	Crystallinity (%)
A	256.9	243.6	261.7	46.8	33% to 41%
B	258.4	230.0	266.7	47.3	33% to 42%
C	252.5	236.2	261.2	47.5	33% to 42%
D	255.0	233.1	262.2	50.3	35% to 45%

As discussed in the Introduction (section 1.9), the percent crystallinity of a semicrystalline polymer can be approximated by using **equation 13:**

$$\% \text{ Crystallinity} = (\Delta H_f/\Delta H^*_f) \times 100 \qquad (13)$$

where ΔH_f is the heat of fusion for the sample, and ΔH^*_f is the heat of fusion for a hypothetical 100% crystalline sample. ΔH^*_f values ranging from 113 to 144 Joules per gram (J/g) have been estimated for PET (9). The heats of formation determined by DSC and the percent crystallinity of each base film sample are also included in Table 8. The ΔH_f and percent crystallinity calculations suggest that the base film from Tape D had the highest degree of crystallinity.

The percent crystallinity calculations in Table 8 confirm that the PET base film materials were semicrystalline. Determination of T_g in semicrystalline polymers can be achieved for samples with low levels of crystallinity. As the percent crystallinity increases, it becomes more difficult to detect the glass transition by DSC. Data on the glassy state for PET can be obtained by analyzing quenched samples (22,23).

Thus, DSC was performed on base film samples from each tape that were quenched from the melt to -25°C. Under such conditions, the PET did not have enough time to crystallize and remained amorphous upon cooling (23). Figure 36 represents the DSC curve for the PET base film from Tape B. This curve was typical for quenched samples of base film from all four tapes. At approximately 75°C (transition 1 in Figure 36), an increase in heat capacity due to the glass transition was detected. At about 130°C (transition 2 in Figure 36), the presence of an exotherm indicates that crystallization occurred. Finally, at approximately 255°C (transition 3 in Figure 36), the endotherm indicates that the PET crystals melted. This DSC curve is quite characteristic of PET and has been used for its identification (23).

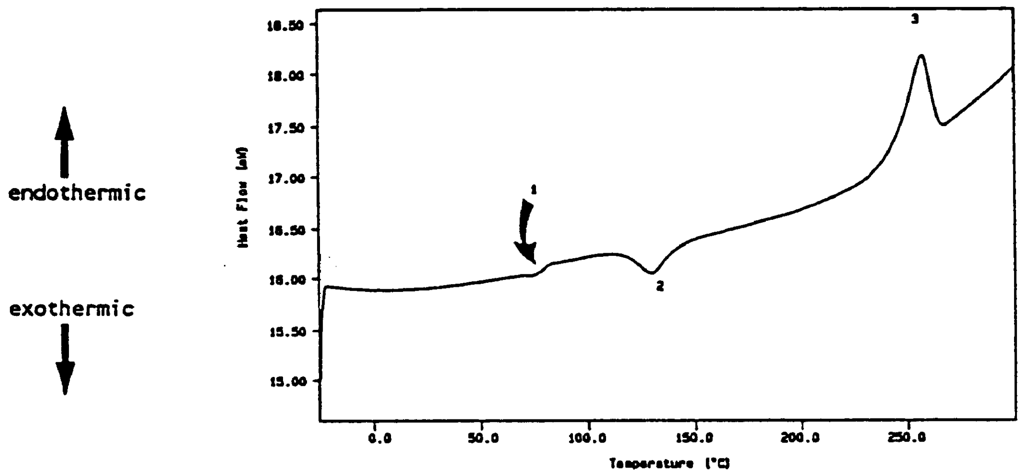

Figure 36. DSC curve for PET base film from Tape B that was quenched prior to analysis. Three transitions were detected. Transition 1 is a glass transition, transition 2 is a crystallization exotherm and transition 3 is a melting endotherm.

The results for the quenched samples of the base films from all four tapes are summarized in Tables 9 and 10. The glass transition and crystallization events are noted in Table 9 and the melting event in Table 10. To describe the glass transition, the inflection point in the heat capacity is listed in Table 8. This temperature closely corresponds to the temperature at which the heat capacity is midway between the liquid and glassy states (T_{gm}). To specify the range of the glass transition, the initiation of the transition (T_{gi}) and the end of the transition (T_{gf}) are also listed. To describe crystallization, Table 9 not only includes the temperature of the peak (T_{cp}), but also the crystallization range identified by an initial temperature (T_{ci}) and a final temperature (T_{cf}). As with crystallization, the temperature of the melting peak (T_{mp}), and the melting range identified by an initial temperature (T_{mi}) and a final temperature (T_{mf}) are listed in Table 10. The transition temperatures listed in Tables 9 and 10 agree with values reported in the literature (10, 22, 23).

Table 9

DSC Results for Quenched Base Film Samples

	Glass Transition			Crystallization		
Tape	T_{gm} (°C)	T_{gi} (°C)	T_{gf} (°C)	T_{cp} (°C)	T_{ci} (°C)	T_{cf} (°C)
A	77.7	75.6	79.3	127.9	121.3	140.3
B	78.9	75.0	82.0	129.5	113.0	151.0
C	77.6	75.4	79.2	125.3	115.1	138.7
D	76.4	73.5	78.2	125.8	116.4	135.0

Table 10

DSC Results for Quenched Base Film Samples

Tape	Melting T_{mp} (°C)	T_{mi} (°C)	T_{mf} (°C)	ΔH_f (J/g)	Crystallinity (%)
A	254.1	245.0	261.3	30.4	21% to 27%
B	257.1	233.0	267.0	32.0	22% to 28%
C	253.6	241.3	260.2	28.9	20% to 26%
D	254.1	244.2	263.4	25.3	18% to 22%

The results in Tables 8 and 10 show negligible differences in melting peak and final melting temperatures. The initial melting temperatures, however, were 1.4 to 11.1°C higher after quenching. This suggests that the variation in crystal size may have been lower for the quenched PET samples (Table 10) compared to the original samples (Table 8). Also, notice the lower ΔH_f values for the quenched base film samples in Table 10. This confirms that additional processes were indeed used to increase the crystalline content of the PET base film used in all four tapes.

Figure 37 shows the DSC curve for a sample of Tape C. The DSC curves for the base film from all four tapes were similar. As with the DSC curve for the PET base film, only one event, an endothermic peak, was observed on this curve. Comparing the peak temperatures in Figures 35 and 37 indicates that the transition identified in Figure 37 also represents the melting of the crystalline portion of the PET base film. No transitions associated with the binder were detected.

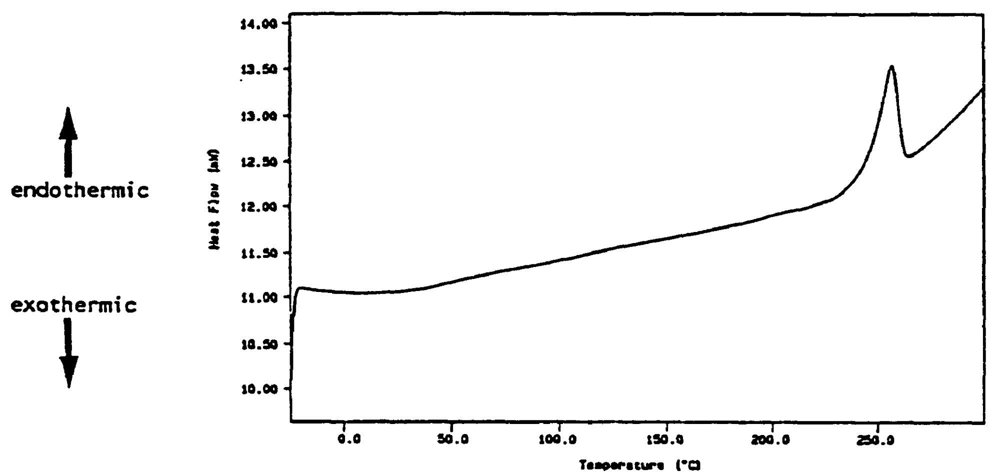

Figure 37. DSC curve for Tape C. Only a melting transition was detected.

Figure 38 presents the DSC curve for Tape C. This curve was typical for quenched samples from all four tapes. As with the DSC curve for the PET base film in Figure 37, three transitions were detected. Comparing the transition temperatures in Figures 35 and 36 indicates that the transitions identified in Figure 38 are associated with the base film and not with the binder. The presence of the magnetic coating on the base film did not markedly influence the glass transition, crystallization and melting temperatures of the base films for the four tapes.

A reason for the absence of transitions for the binder in Figures 37 and 38 is the relatively small weight percent of the binder compared to the whole tape. From Table 7 in section 3.1.8, recall that the weight percent of the binder is less than 4.5 % for Tapes A and C, less than 6.5% for Tape B, and less than 8.6% for Tape D.

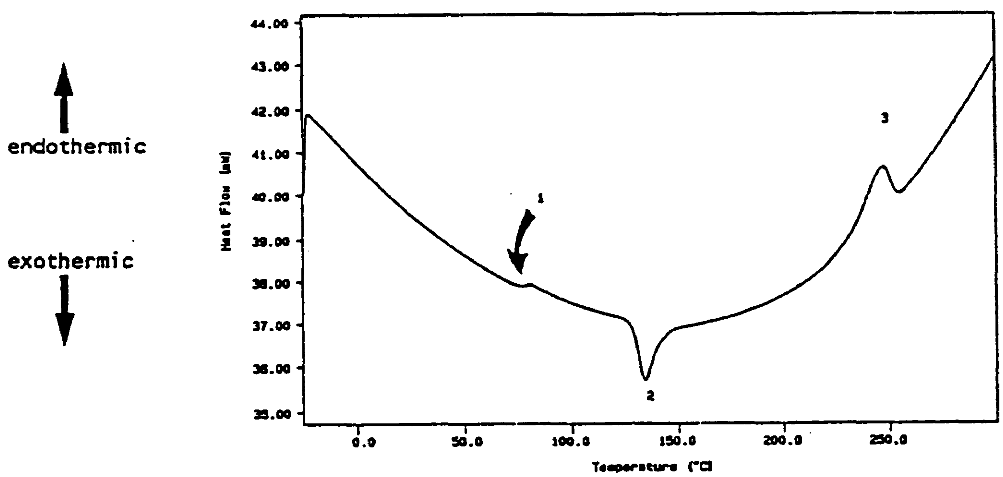

Figure 38. DSC curve for Tape C that was quenched prior to analysis. The three detected transitions (labelled 1, 2 and 3) are all associated with the base film.

Finally, the coating samples that were scraped from each tape did not display any transitions. It was expected that transitions associated with the binder would be detected from the coating samples. One reason for not detecting binder transitions may have been the small sample size. Since the coating samples were in the form of shavings, only a small quantity amounting to less than 1.75 mg could be added to a DSC sample pan. From Table 7 in section 3.1.8, the weight of the magnetic particles relative to the weight of the binder is on the order of 2 or 3 to 1 depending upon the tape. Thus, the total weight of the binder in each coating sample was probably less than 0.5 mg. Such a small sample may not have been adequate for DSC analysis.

3.2.2 TMA of Base Films and Magnetic Tapes.

Thermomechanical analysis (TMA) was used to examine observable transitions of each base film and magnetic tape by monitoring deformation with increasing temperature at a constant rate while under a fixed load. TMA curves for the base film from Tape B tested in extension under three different static loads (50 mN, 250 mN and 500 mN) are shown in Figures 39, 40 and 41. A summary of the results from these three curves is presented in Table 11.

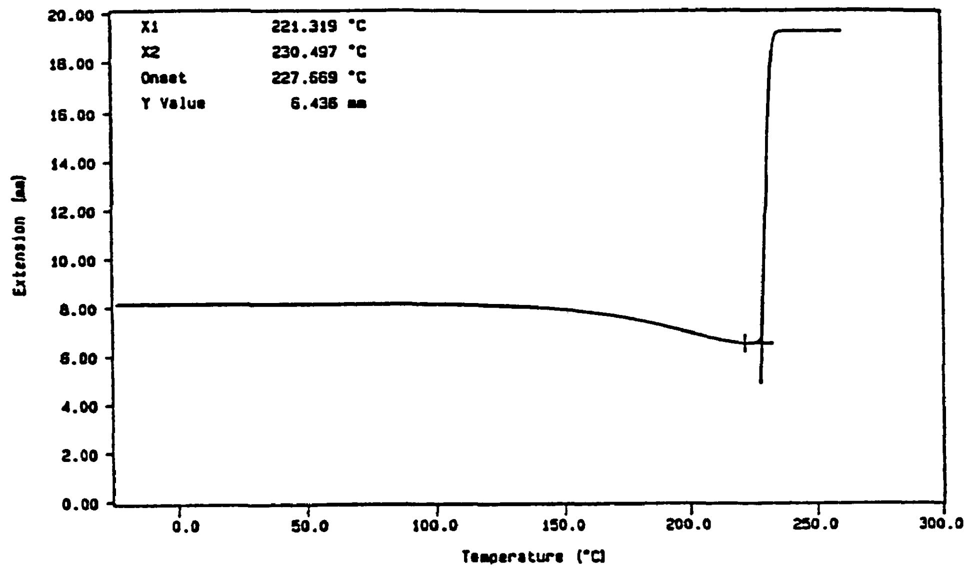

Figure 39. TMA curve of the base film material from Tape B under a fixed load of 50 mN. Volume contraction is represented by a decrease in the grip position and volume expansion by an increase in grip position. The expansion onset calculation is included.

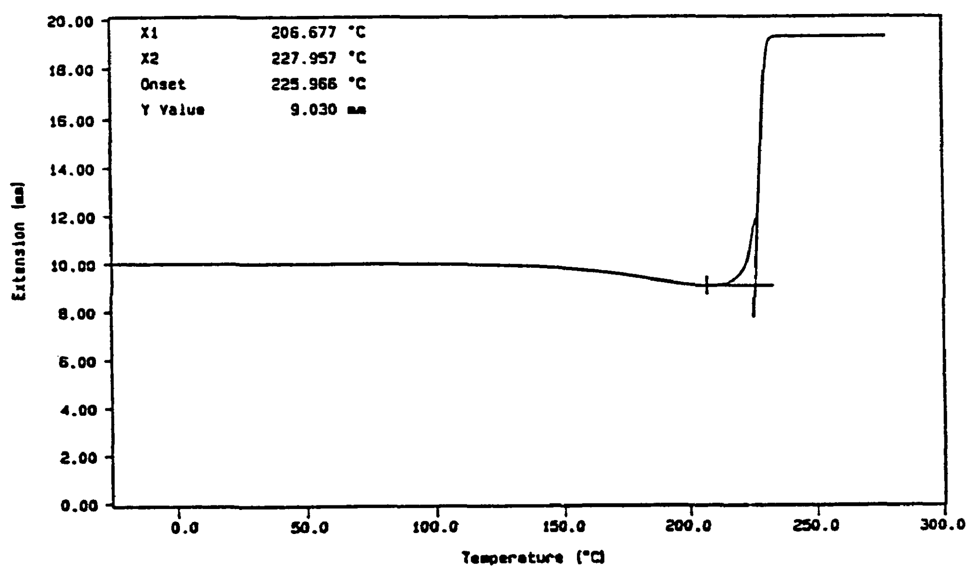

Figure 40. TMA curve of the base film material from Tape B under a fixed load of 250 mN. Volume contraction is represented by a decrease in the grip position and volume expansion by an increase in grip position. The expansion onset calculation is included.

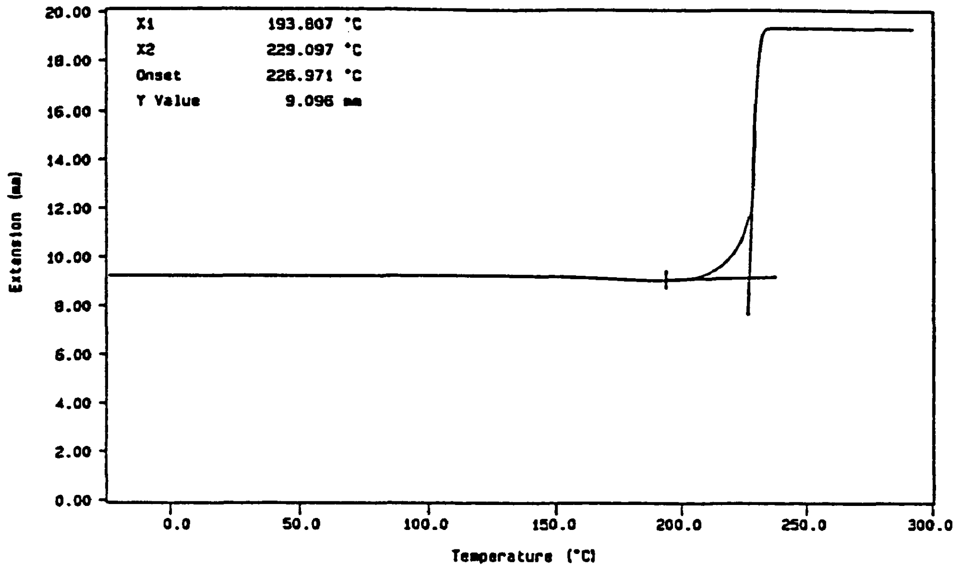

Figure 41. TMA curve of the base film material from Tape B under a fixed load of 500 mN. Volume contraction is represented by a decrease in the grip position and volume expansion by an increase in grip position. The expansion onset calculation is included.

Concentrating on Figure 39, the height of the upper extension grip used to hold the specimen remained relatively constant until approximately 125°C. At that temperature a noticeable decrease in the original grip height was observed, indicating that the base film sample shrank. Since crystallization is associated with volume contraction, the observed shrinking provided evidence that additional crystallization occurred in the base film sample. Above 150°C the shrinking became more significant. The initial shrinking temperature of approximately 125°C agreed with the crystallization temperatures determined by DSC in section 3.2.1 for quenched PET.

In Figure 39, at approximately 224°C the grip position began to increase as the base film sample started stretching. At 228°C there was a significant increase in grip position over a temperature range of only a few degrees. This indicated that the base film sufficiently melted allowing the sample to break apart under a static loading condition of 50 mN.

The data in Table 11 shows that the temperature, at which contraction of the base film began, increased as the static loading increased. In addition, the amount of contraction decreased (denoted in Table 11 by negative changes in grip height) as the static loading increased. This was because the direction of the static load applied to the sample directly opposed the direction of volume contraction in the sample.

Table 11 also lists approximate temperatures at which initial expansion was evident and the expansion onset temperature. The expansion onset temperature was defined as the intersection point of the extrapolated baseline where expansion first began with the tangent of the inflection in the TMA curve. The tangent of the inflection in the TMA curve was identified by a peak in the first derivative.

Notice in Table 11 that as the static load increased, the temperature at which initial expansion was observed in the base film decreased. The onset temperatures shown in Table 11, however, remained approximately the same.

Table 11

TMA Results of Tape B Base Film Under Three Different Static Loading Conditions

	Static Load		
	50 mN	250 mN	500 mN
initial contraction:	125°C	140°C	175°C
Δ grip height due to contraction:	-20.4%	- 9.4%	- 2.3%
initial expansion:	224°C	208°C	193°C
expansion onset:	228°C	226°C	227°C

The base films from Tapes A, C and D were evaluated only under a static loading condition of 50 mN, because 50 mN best approximated a zero loading condition when taking into account the expansion test fixtures. The TMA curves for the base films from Tapes A, C and D, while under a static load of 50 mN, resembled Figure 39. Table 12 summarizes these results. The results were relatively similar for all four tapes with the exception of the change in grip height due to contraction. The relative decrease in grip height was only 13.6% for the base film from Tape D, but ranged from 18.3% to 20.4% for the other three tapes. This means that the base film for Tape D was stiffer and more stable up to temperatures as high as 219°C. This response was accepted because the DSC results in section 3.2.1 indicated that the base film for Tape D had a higher degree of crystallinity than the other three tapes. Notice that volume expansion due to the glass transition was not detected in the base film samples. The highly crystalline structure of these films most likely impeded the detection of the glass transition temperature. Finally, the data in Tables 11 and 12 indicated that TMA is more sensitive than DSC for detecting crystallization temperatures of the semicrystalline PET base films. Recall that crystallization temperatures of the semicrystalline base film samples were not detected by DSC.

Table 12

TMA Results of Base Film from Each Tape Under a Static Load of 50 mN

Tape	Δ grip height due to contraction (%)	initial expansion (°C)	expansion onset (°C)
A	-19.6	217	222
B	-20.4	224	228
C	-18.3	217	223
D	-13.6	216	221

The TMA curve for a sample of magnetic tape (Tape A) tested in extension under a static load of 50 mN is shown in Figure 42. Comparing this figure with Figure 39, first note that the scales are different. Secondly, there is no increase in grip position spanning 10 mm as in Figure 39. Finally, the maximum temperature recorded in Figure 42 was 342°C versus approximately 250°C in Figure 39. These observations indicate that the magnetic tape sample remained in tact up to 342°C. At 342°C the tape suddenly broke apart. The increase in grip height was not plotted because the TMA instrument was not designed to detect such rapid increases in grip height. The addition of binder and magnetic particles to the tape provided enough support so that the tape did not separate at the melting point of the base film material.

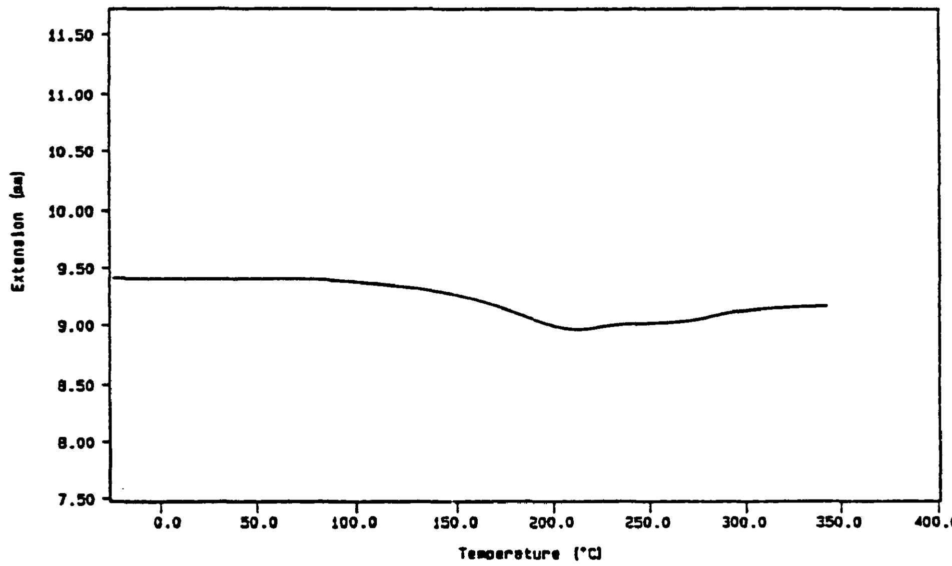

Figure 42. TMA curve of Tape A under a fixed load of 50 mN. Volume contraction is represented by a decrease in the grip position and volume expansion by an increase in grip position.

Table 13 summarizes the TMA results for all four magnetic tapes under a static load of 50 mN. The TMA curves for all four magnetic tapes were similar with the exception of the temperature at which the tape broke. The breaking temperature for the tapes ranged from 342°C for Tape A to 398°C for Tape D. A possible reason for the higher breaking temperature for Tape D is that this tape was coated with binder and magnetic particles on both sides. This may have provided the extra support to hold the tape together for an additional 40 to 50°C.

Table 13

TMA Results of Each Magnetic Tape Under a Static Load of 50 mN

Tape	Δ grip height due to contraction (%)	initial expansion (°C)	breaking point (°C)
A	- 4.7	209	342
B	- 3.1	212	355
C	- 3.1	209	352
D	- 2.9	206	398

Table 13 also shows that the initial expansion temperatures for the magnetic tapes ranged from 206°C for Tape D to 212°C for Tape B. These initial expansion temperatures are lower that those for the base film materials. It appears that the initial expansion was caused by movement of the binder.

Table 13 also indicates that the relative decrease in grip height ranged from 2.9% for Tape D to 4.7% for Tape A. This indicates that Tape D is stiffer than the other three tapes. The enhanced stiffness may not only be due to the base film material, but also because Tape D was coated with binder and magnetic particles on both sides.

3.2.3 DMA of Base Films and Magnetic Tapes.

The thickness of each tape, base film and coating were determined as a prelude to the DMA experiments. These results are presented in Table 14. This table indicates that the measured thickness of the four base films were equivalent, but that there was some variation in the total thickness of each tape. The thickest tape was Tape D, which had both a front and back coat over the base film. The top coating thickness ranged from 3.4 μm for Tape B to 3.9 μm for Tape D. The thickness values listed in Table 14 for the base films and for each tape were used in the determination of the magnitudes for the derived DMA parameters.

Table 14

Tape, Base Film and Coating Thickness

Tape	Total Thickness (μm)	Base Film (μm)	Top Coating (μm)	Bottom Coating (μm)
A	29.7	26.0	3.7	0
B	29.4	26.0	3.4	0
C	30.5	26.0	3.5	1.0
D	29.9	26.0	3.9	0

Figure 43 shows the DMA results of the PET base film for Tape D. Included in this figure are curves for the storage modulus (E'), loss tangent (tan δ) and the loss modulus (E′′). Individual curves for each parameter are shown in Figures 44, 45 and 46 respectively. The DMA curves for the base film materials for the remaining tapes were similar to those shown in Figures 43 through 46.

In Figure 44 the E′ curve for Tape D had a magnitude of 3.4 x 10^9 at -25°C. The magnitude decreased as the temperature increased. At approximately 77°C, there was a sharp decrease in the modulus. This temperature corresponds closely to the glass transition midpoint temperature of the PET base film as determined by DSC (78.8°C). The sharp decrease in E′ was caused by the free volume expansion associated with the glass transition. At approximately 125°C the modulus began to level off. It was at this temperature that shrinking was observed in the PET base film by TMA.

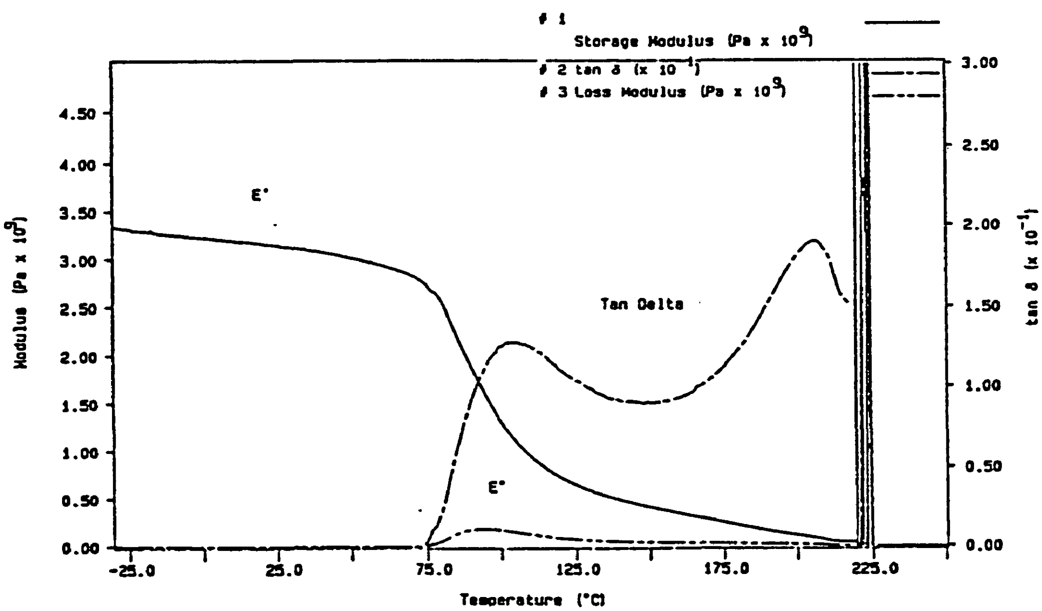

Figure 43. DMA curves of the PET base film for Tape D. Included are curves for E′, E′′ and tan δ.

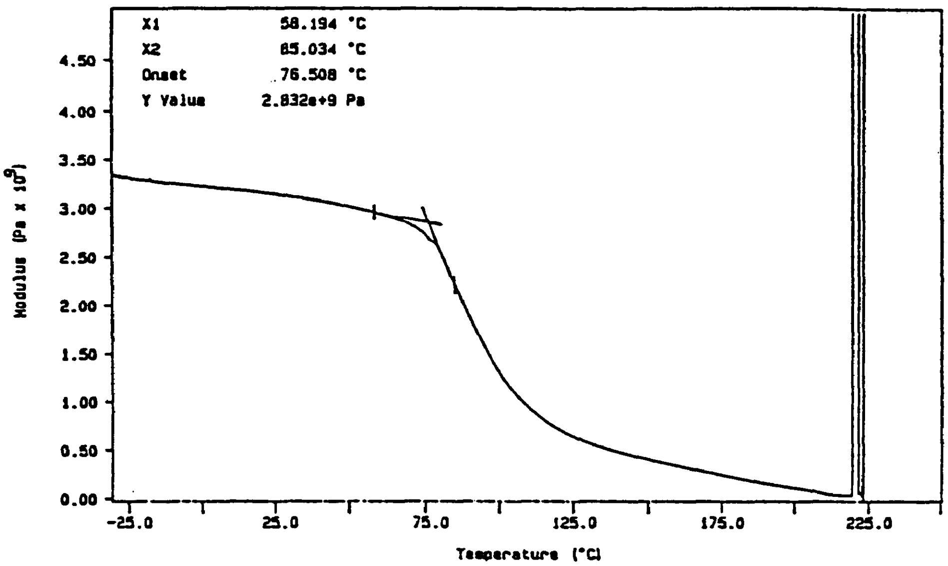

Figure 44. E′ curve of the PET base film for Tape D.

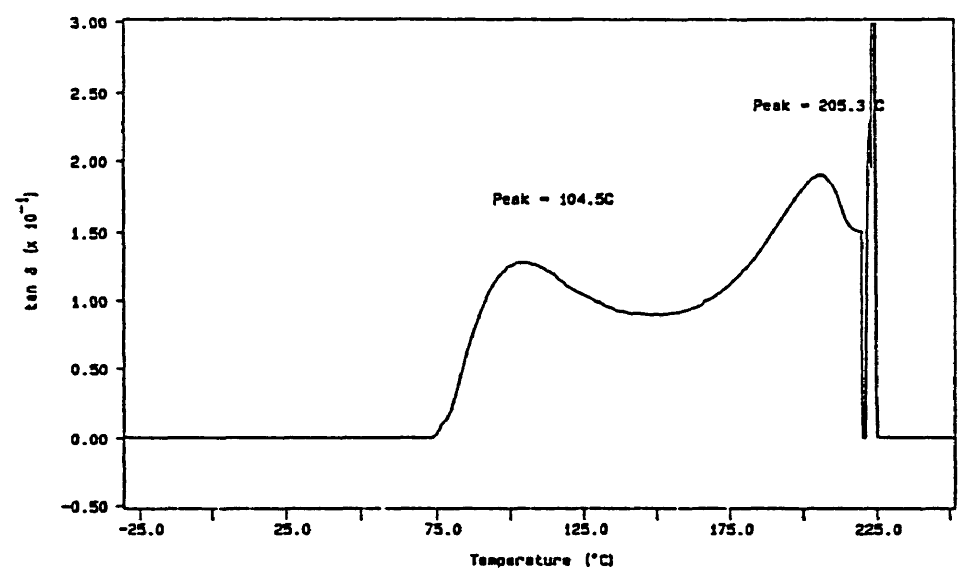

Figure 45. Tan δ curve of the PET base film for Tape D.

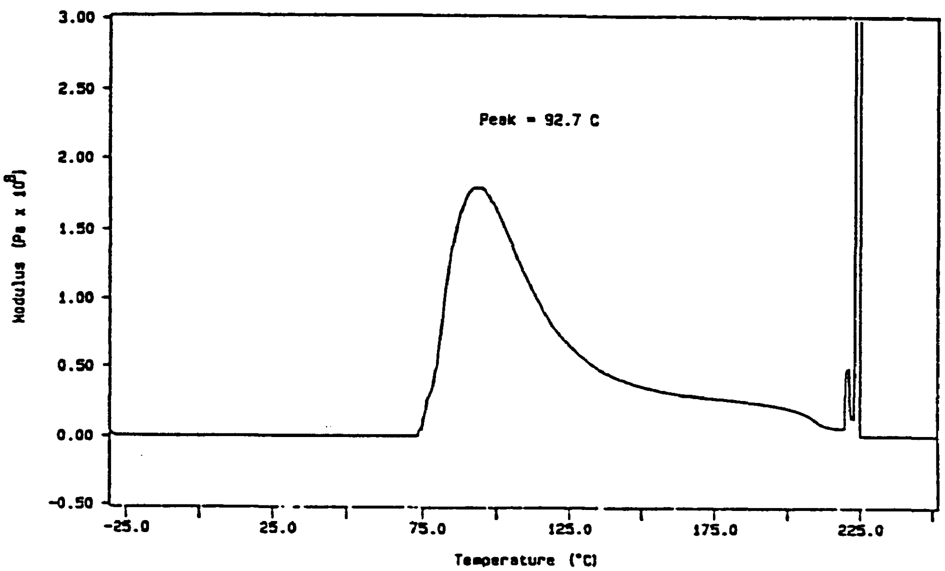

Figure 46. E'' curve of the PET base film for Tape D.

In Figure 45, the magnitude of the tan δ curve for the base film from Tape D was near 0 from -25°C up to approximately 73°C where it began to rise. This temperature was only 2°C lower than the temperature which marked the initiation of the glass transition for the base film as detected by DSC (see Tables 8 and 9). At 73°C, the tan δ curve began to rise up to a peak temperature of 105°C with a peak magnitude of 0.128. After the maximum, the tan δ curve decreased until approximately 150°C where the curve increased again to a second peak at 205°C with a peak magnitude of 0.191. Finally, at about 225°C the base film broke causing the sharp increase in tan δ. The melting point as detected by DMA was approximately 25°C lower than that detected by DSC. The lower DMA melting temperature for the base film was probably caused by the dynamic loading condition.

In Figure 46, notice that the E'' curve for the base film from Tape D initially parallelled the tan δ curve for the same tape shown in Figure 45. The E'' curve was approximately 0 from -25°C up to 73°C where it began to rise. A peak was reached at an approximate temperature of 93°C with a peak magnitude of 1.8×10^8. Comparing Figures 44 and 46, note that E'' reached its maximum at a temperature near the inflection point in E'. Also, note that E'' reached a maximum at a slightly lower temperature than the tan δ peak. After the maximum in Figure 46, the E'' curve decreased. No second peak was identified until the jump at 225°C, which was caused by expansion of the base film resulting in failure.

Table 15 presents the DMA transition temperature results for the PET base film of all four tapes. Included in this table are the initial temperatures at which deviation in the baseline occurred and the peak temperatures for both tan δ and E''. The onset temperatures and inflection points in the E' curves are also included.

Table 15

DMA Transition Temperature Results for the Base Film in °C

	tan δ		E''		E'	
Tape	initial	peak	initial	peak	onset	inflection
A	70.3	108.6	70.3	94.8	72.0	91.1
B	72.5	114.3	72.5	99.6	78.2	99.6
C	67.5	105.0	67.5	92.7	76.7	91.3
D	72.9	102.2	72.9	94.8	76.9	95.0

Table 16 presents the magnitudes of the thermomechanical transitions associated with the PET base film from the four tapes. Included are the magnitudes of the peaks from the tan δ and E'' curves, the magnitudes of the inflection point in the E' curve, and the magnitudes of E' at 25°C.

Table 16

Magnitude of DMA Peaks for the Base Films

Tape	tan δ peak	E'' peak (Pa)	E' at 25°C (Pa)	E' onset (Pa)
A	0.150	2.3×10^8	3.0×10^9	2.8×10^9
B	0.153	2.2×10^8	3.3×10^9	2.9×10^9
C	0.127	1.8×10^8	3.0×10^9	2.5×10^9
D	0.128	1.8×10^8	3.2×10^9	2.7×10^9

In Table 15, notice that the temperatures at which the tan δ and the E'' curves began to deviate from 0 and the onset temperatures of the E' curve correlate with the glass transition values reported by DSC in Table 9. The presence of all three events confirm the existence of a major thermomechanical transition.

The second peak in the tan δ curve is not supported by the presence of an E'' peak or a sudden change in E'. This second peak appears to be caused by the continuous drop in E'. Recall from **equation 31** in section 1.11 that tan δ = E''/E'. This equation suggests that a decrease in E' or an increase in E'' causes tan δ to increase. The increase in tan δ is enhanced by the order of magnitude difference between the E'' peak and the E' inflection as shown in Table

16. If it were not for the shrinking of the base film as verified by TMA, the tan δ peak may have continued to rise creating a single peak instead of two separate peaks.

Table 16 includes the magnitude of E′ at 25°C for the base film of each tape so that E′ can be compared at the same temperature. Recall from section 3.2.1 that the base film from Tape D had the highest degree of crystallinity. With the exception of the base film from Tape B, the results suggest that E′ increases with increasing degrees of crystallinity. Averaging the results from multiple samples may confirm this observation.

Notice in Figures 45 and 46 that no secondary damping peaks were detected below the events associated with the glass transition temperature of the base film. Such peaks would be associated with side chain motion. The absence of such peaks is consistent with the highly linear structure of PET.

Table 17 shows a summary comparison of the base film transitions as detected by DSC, TMA and DMA. The DSC results were taken from Tables 9 and 10 for quenched samples of the base films. Recall that only T_m was originally detected by DSC on the semicrystalline PET base film samples. The T_g values determined by DSC in Table 17 for each tape represent the temperature range over which the glass transition occurred. The reported T_c and T_m values by DSC in this table were the peak temperatures. The T_g was not detected by TMA and only an approximation of T_c can be made. The T_m values by TMA in Table 17 were the expansion onsets reported in Table 11. The DMA T_g values reported in Table 17 specify a range as determined by the initial deviation from the baseline for the loss factors (tan δ and E'') and the onset value for E'. Only an approximation could be made for T_c by DMA. The reported T_m by DMA for each base film in Table 17 is the temperature at which the base film failed in expansion.

In Table 17, notice the close correlation between the T_g values determined by DSC and DMA. The T_c values determined by DSC and TMA were also comparable. Finally, the T_m values determined by TMA and DMA were similar.

Table 17

Comparison of Transition Temperatures of Base Films as Detected by DSC, TMA and DMA

	T_g (°C)	T_c (°C)	T_m (°C)
DSC:			
Tape A	75.6 - 79.3	127.9	254.1
Tape B	75.0 - 82.0	129.5	257.1
Tape C	75.4 - 79.2	125.3	253.6
Tape D	73.5 - 78.2	125.8	254.1
TMA:			
Tape A	not detected	~125	222
Tape B	not detected	~125	228
Tape C	not detected	~125	223
Tape D	not detected	~125	221
DMA:			
Tape A	70.3 - 72.0	~150	225
Tape B	72.3 - 78.2	~150	228
Tape C	67.5 - 76.7	~150	223
Tape D	72.9 - 76.9	~150	228

Figure 47 shows the DMA results of Tape B. Included in this figure are curves for E′, tan δ and E′′. Individual curves for each parameter are shown separately in Figures 48, 49, and 50 respectively.

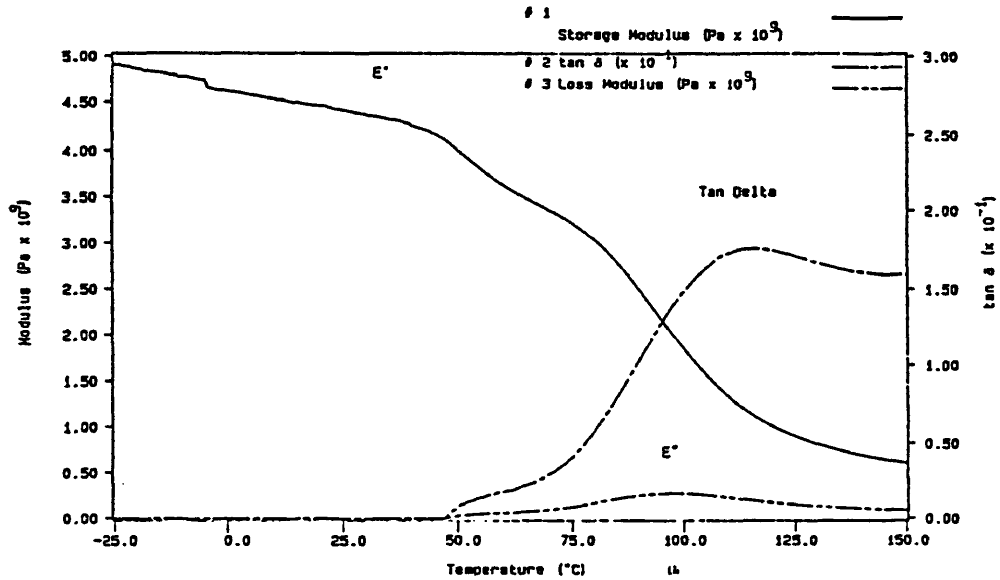

Figure 47. DMA curves for Tape B. Included are curves for E′, E′′, and tan δ.

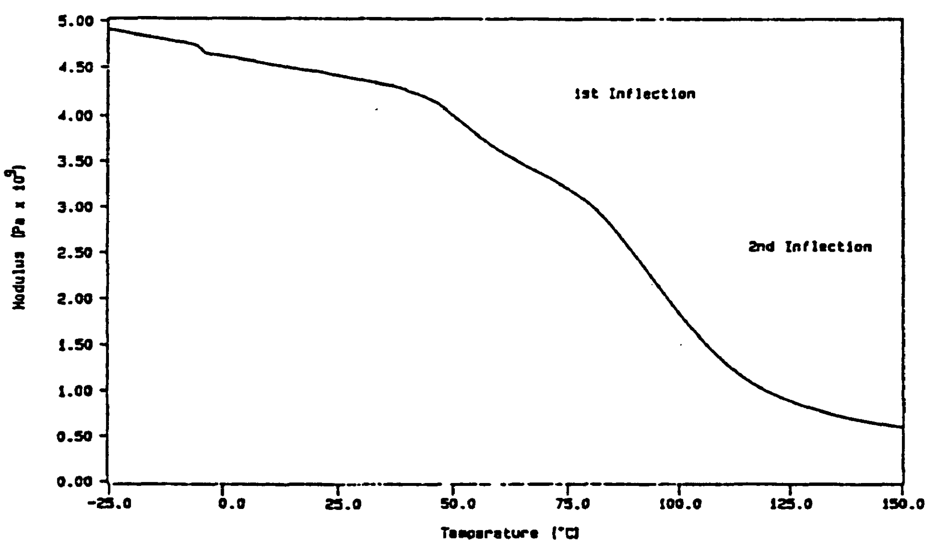

Figure 48. E′ curve for Tape B.

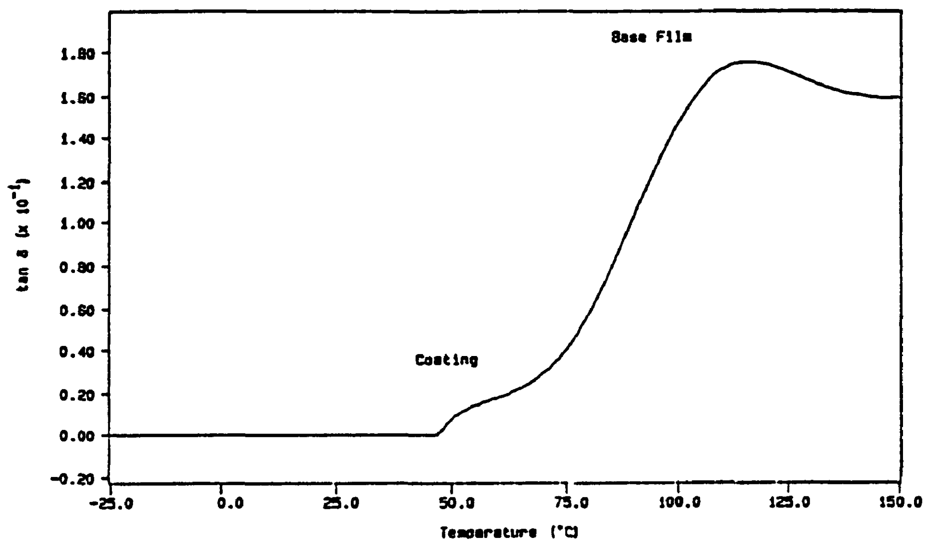

Figure 49. Tan δ curve for Tape B.

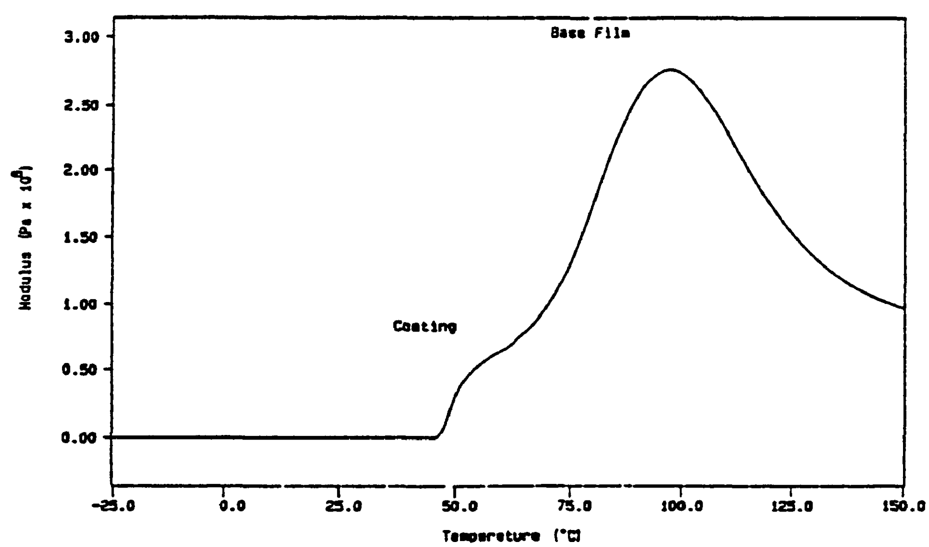

Figure 50. E'' curve for Tape B.

In Figures 49 and 50 notice the presence of the hump at approximately 50°C. Other than this hump, the remaining shape of the tan δ and E'' curves were similar to those for the base film in Figures 45 and 46. This hump was caused by a thermomechanical transition associated with the magnetic coating. In addition, the E' curve in Figure 48 shows two inflection points, which support the existence of two different thermomechanical transitions.

Although the DMA curves for the remaining tapes were similar to those shown in Figures 47 through 50, there were significant differences, particularly with respect to the temperatures at which the baselines began to deviate. To facilitate comparison, Table 18 lists the DMA transition temperature results associated with the binder of each tape. The values reported in Table 18 are averages based on three test samples from each tape. The standard deviation is shown in parentheses below each average value.

Table 18 indicates that Tapes A, B and C had tan δ and E'' peak temperatures associated with the binder ranging from 55 to 62°C. As with the base films, the tan δ peaks for the binders occurred at slightly higher temperatures than their corresponding E'' peaks. No peaks in tan δ and E'' associated with the binder could be clearly distinguished for Tape D.

It is possible that relaxations associated with the back coat from Tape D interfered with the thermomechanical response of its top coat.

Table 18

DMA Transition Temperatures for Whole Tapes in °C

	tan δ		E''		E'	
Tape	initial	peak	initial	peak	onset	inflection
A	18.5 (3.1)	56.0 (2.0)	-9.1 (3.4)	55.2 (2.0)	*	46.4 (1.3)
B	49.3 (2.9)	61.9 (1.8)	49.0 (2.9)	57.8 (2.2)	46.6 (1.3)	53.4 (1.2)
C	40.0 (4.1)	61.1 (2.2)	39.4 (4.4)	59.6 (2.4)	43.5 (2.0)	52.9 (0.2)
D	5.9 (3.8)	*	6.3 (3.3)	*	*	*

values in parentheses are standard deviations
* - not clearly distinguishable

Although the peak temperatures in Table 18 only differed by 5 to 6°C for Tapes A through C, the temperatures at which the E'' and tan δ curves began to deviate from the baseline differed by as much as 58°C. The E'' curves for Tapes A, C, and D are shown in Figures 51 through 53 respectively for comparison with that for Tape B in Figure 50. At one extreme, the E'' curve for Tape B began to deviate from the baseline at 49°C. At the other extreme, the curve for Tape A began to deviate from the baseline at -9.1°C. These variations are significant because they range from subambient to above room temperature.

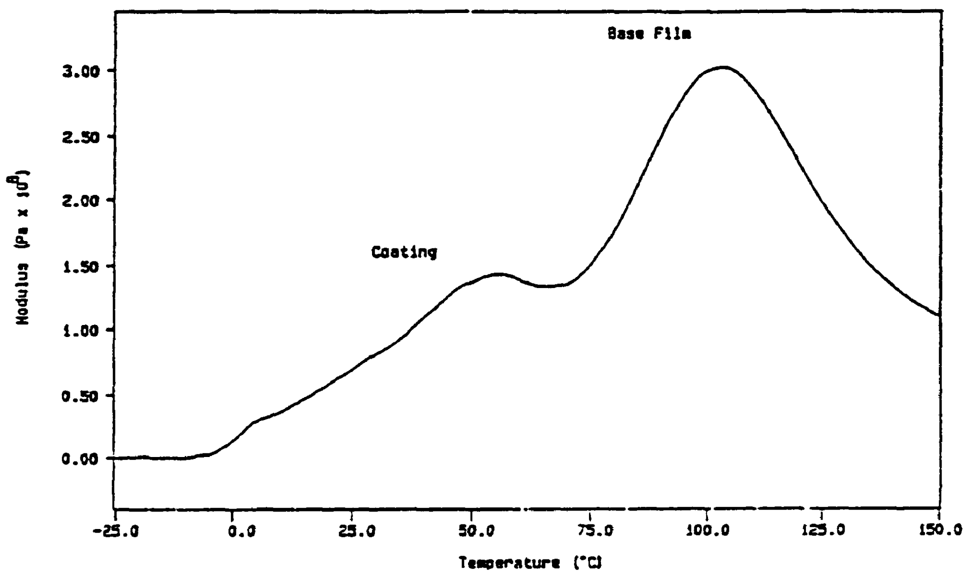

Figure 51. E'' curve for Tape A. The baseline began to deviate at approximately -9°C.

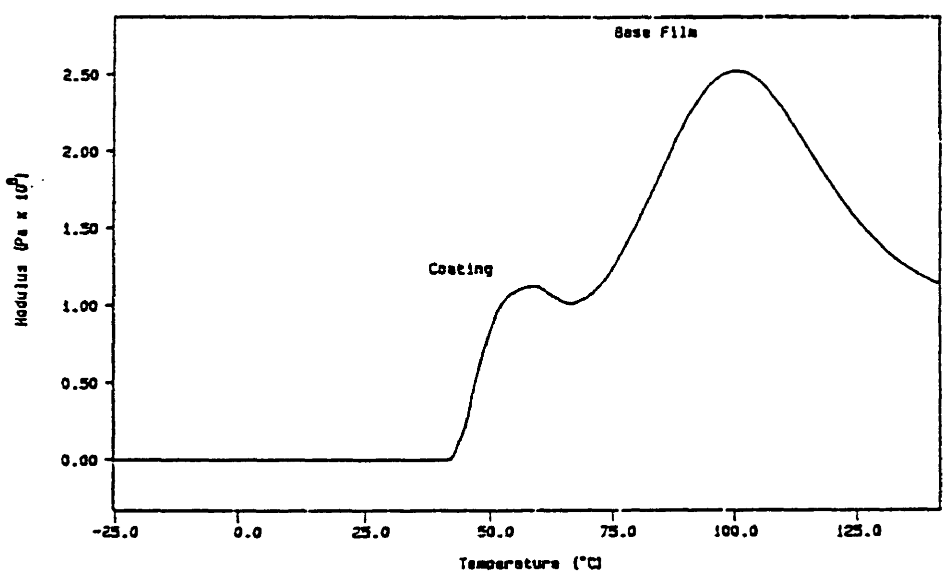

Figure 52. E'' curve for Tape C. The baseline began to deviate at approximately 39°C.

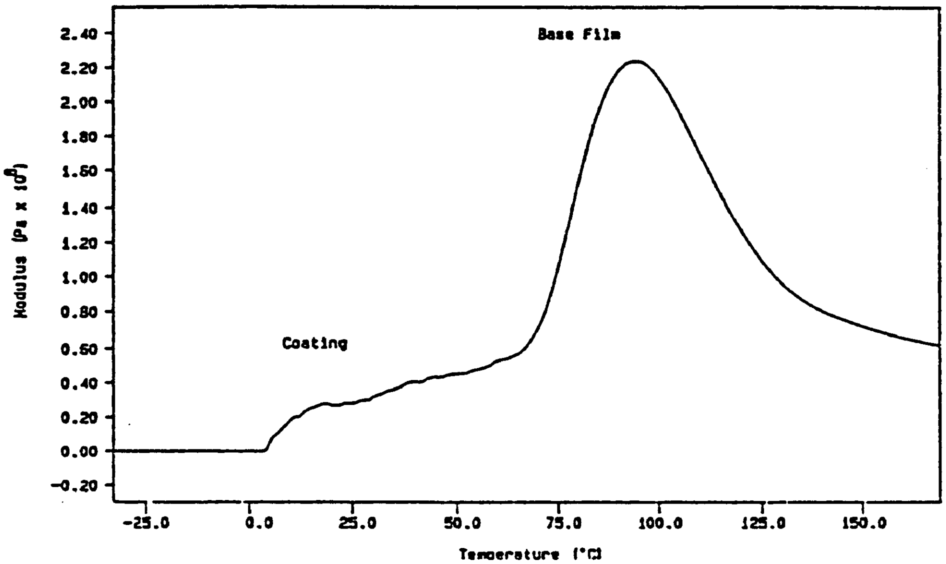

Figure 53. E'' curve for Tape D. The baseline began to deviate at approximately 6°C.

Table 19 presents the magnitudes of the thermomechanical transitions associated with the binders from each tape. Note that Tape A, which displayed the lowest initial transition temperature associated with the binder, also displayed the highest peak values for the loss factors (tan δ and E''). Tape B, which displayed the highest initial binder transition temperature, displayed the lowest peak values for the loss factors. There appears to be a correlation between the initial transition temperature associated with the binder and the magnitude of the loss factor peaks. The lower the initial transition temperature, the greater the magnitude of the loss factor peak.

Table 19

Magnitude of DMA Peaks for the Magnetic Tapes

Tape	tan δ peak	E'' peak (Pa)	E' at 25°C (Pa)	E' onset (Pa)
A	0.038 (0.002)	1.4×10^8 (0.5×10^8)	4.8×10^9 (0.4×10^9)	4.2×10^9 (0.3×10^9)
B	0.018 (0.001)	0.6×10^8 (0.2×10^8)	4.8×10^9 (0.6×10^9)	4.2×10^9 (0.5×10^9)
C	0.029 (0.002)	1.1×10^8 (0.6×10^7)	5.3×10^9 (0.3×10^9)	4.3×10^9 (0.2×10^9)
D	*	*	3.6×10^9) (0.4×10^9)	*

* - not clearly distinguishable

Table 19 also indicates that the E' values at 25°C for all four magnetic tapes were greater than their counterparts for the base film shown in Table 16. Thus, the addition of the magnetic coating has a significant effect on E', ranging from an increase in magnitude of 13% for Tape D to 43% for Tape C.

In section 1.3 of the Introduction, the binder was described as a block copolymer containing polyester soft segments connected to polyurethane hard segments. The literature indicates that both the soft and hard segments can reside in a semicrystalline state (5,7,14,15). That is, both segments have a glass transition associated with the amorphous regions of the polymer and a melting temperature associated with the crystalline regions. Peaks in the loss factors for the binder indicated the existence of a transition in the temperature range of 55 to 62°C depending upon the magnetic tape. DMA did not, however, decipher the type of transition. A comparison of literature values (5,14) with the DMA peak transition temperatures for the binder suggested that the observed DMA transition was most likely associated with the melting of the polyester soft segment.

Recall from section 1.3 that the polyurethane hard segments associate through strong hydrogen bonds and dipole-dipole interactions. This causes the hard segments to aggregate into domains surrounded by the soft segment phase. Crystallinity of the soft segment phase as well as increased miscibility with the hard segments has been reported to increase the overall softening point of the binder. This is caused by a reduction in the interaction between the hard segment blocks (7). The onset of melting of the crystalline soft segment phase at or below room temperature can only reduce the overall softening temperature of the binder.

Several factors have been suggested in the literature to influence the melting point of the soft segment. Increasing the ratio of hard segment to soft segment has been reported to enhance restriction of the soft segments thereby increasing their melting point (14, 15). A study by Bradshaw and Bhushan indicated that interaction of the binder with the relatively small magnetic particles shifted the thermomechanical transitions to higher temperatures (5). Thermal aging of magnetic tape has been observed to increase the thermomechanical response of the soft segment. It was suggested that the higher temperature produced an increase in binder interaction with the magnetic particles (5). As described in section 1.6, degradation of the binder can affect the thermomechanical response of the soft segments. It is also conceivable that process problems can influence the binder's thermomechanical transition temperatures.

Regardless of these factors, the variations in initiation of the loss factors for the binder from each tape were significant. Recall that the initiation temperatures of the loss factors for the binders from each tape varied from -10 to 55°C. This variation was more extreme than the differences in peak temperatures of the loss factors. From section 1.11, E'' was said to express a material's ability to dissipate mechanical energy by converting it to heat through molecular motion, and that an increase in tan δ implies increased viscous behavior. Those tapes with binders that showed evidence of increases in the loss factors at ambient or subambient temperatures, such as Tape A and D, have an increase in molecular motion at room temperature. Increased mobility of the soft segments for a particular tape would only seem to enhance its potential for stiction related problems.

Chapter 4

CONCLUSIONS

Through the use of a variety of analytical techniques, the major components of four different magnetic tape used in computers were characterized. The techniques used in this study, the components analyzed by each technique, and the findings are summarized in Table 20.

The GC/FTIR/MS results indicated that the lubricants from all four tapes contained fatty acids and fatty acid esters. Tapes A and D also contained a difunctional ester.

Results from the ESCA technique provided evidence that the magnetic coating contained chromium dioxide (CrO_2) and organic compounds. The SEM photomicrographs indicated that this coating consisted of highly oriented acicular particles. To determine particle sizes, the binder would have to be removed by a technique such as plasma etching. The DMA data showed that the addition of the magnetic coating to the base film significantly increased the magnitude of E′ at room temperature.

Table 20

Summary of Findings

Technique	Component Studied	Tapes	Findings
GC/FTIR/MS	lubricants	all	fatty acids, fatty acid esters
		A,D	difunctional ester
FTIR	base film	all	PET
	binder	all	polyester-polyurethane
ESCA	magnetic coating	all	chromium dioxide, organic compounds
SEM/EDS	magnetic coating	B	chromium-oxygen rich acicular particles
Gravimetric	base film	all	76.6 to 80.4 weight %
	chromium dioxide	all	14.5 to 16.0 weight %
DSC	base film	all	detected T_g, T_c, T_m
	binder	all	no transitions detected
TMA	base film	all	detected T_c, T_m
	binder	all	no transitions detected
DMA	base film	all	detected T_g, T_c, T_m
	binder	all	detected T_m of polyester soft segment

FTIR analysis of the base films from the four tapes indicated that PET was used exclusively. The crystallization and melting transitions of the four PET base films were detected by DSC, TMA and DMA. DSC clearly defined a crystallization temperature range for the base films, whereas TMA and DMA yielded only approximations. The melting temperatures of the base films determined by TMA and DMA were about 25°C lower than those determined by DSC. This was due to the loading conditions required by the TMA and DMA techniques. The glass transition of the base films, however, was detected only by DSC and DMA. DSC was not sensitive to the glass transition of the semicrystalline PET base films. Only after quenching, was the glass transition detected. DMA was capable of detecting the glass transition of the base film as confirmed by the existence of peaks in both tan δ and E'', and by the existence of an inflection point in E'. It was, however, the temperatures at which the tan δ and E'' baselines began to deviate, and the expansion onset temperature that corresponded closely to the glass transition temperature ranges of the base films as determined by DSC.

Through the use of gravimetric methods, it was possible to approximate the relative percentages of base film and CrO_2 in each tape. Determining the percentage of CrO_2 by TGA required the incorporation of a correction factor to account for the loss of oxygen during the TGA experiments.

FTIR analysis of the acetone soluble residues from each tape indicated that the binders were all polyester-polyurethane systems. The isocyanate active component of the system used in all four binders was fully reacted. Of the three thermal transition analysis techniques used, only DMA was able to detect a transition associated with the binder. The DMA data showed that the binders were sensitive to elevated temperatures. Peak values for the loss factors of the single coated tapes (Tapes A, B and C) indicated that the binder transition ranged from 55 to 62°C. Initiation of the loss factors, however, ranged from -9 to 49°C. It was suggested that this transition was associated with the melting of the polyester soft segments. The differences between the initiation and peak temperatures of the loss factors for Tapes A and D suggest that relaxations associated with the melting of the soft segments can occur over a wide temperature range. It is possible that relaxations associated with the back coat on Tape D interfered with the thermomechanical response of the top coat. Therefore, the DMA method may only be valid for magnetic tapes without back coats.

The development of a new DMA method capable of obtaining repeatable data is of value to manufacturers of tape storage devices as well as tape manufacturers. Increased mobility of the binder due to the melting of the polyester soft segments at or below room temperature provides additional insight to reasons why some magnetic tapes may be more prone to stiction related problems than other tapes.

Finally, the base film of Tape D appeared to have the better overall physical and mechanical properties for use in magnetic tape. As shown in Table 20, it had the highest degree of crystallinity, exhibited the least amount of contraction, displayed the least amount of dampening, and had a relatively high modulus. As for performance of the binder, the DMA results suggest that Tape A would be the most likely of the four tapes to have binder problems associated with it and Tape B the least likely.

Table 21

Comparison of Thermal Analysis Results

	Tape A	Tape B	Tape C	Tape D
Base Film:				
% crystallinity (DSC)	33-41%	33-42%	33-42%	35-45%
contraction (TMA)	19.6%	20.4%	18.3%	13.6%
tan δ peak magnitude (DMA)	0.150	0.153	0.127	0.128
E′ at 25°C (x 10^9) (DMA)	3.0	3.3	3.0	3.2
degradation onset (TGA)	407°C	416°C	417°C	415°C
Binder:				
initial tan δ deviation (DMA)	18.5°C	49.3°C	40.0°C	5.9°C
initial E′′ deviation (DMA)	-9.1°C	49.0°C	39.4°C	6.3°C

REFERENCES CITED

1. Jorgensen, F. "The Complete Handbook of Magnetic Recording", 3rd ed.; TAB Books: Blue Ridge Summit, Pennsylvania, 1988.

2. "Encyclopedia of Chemical Technology"; John Wiley & Sons: New York, 1981; Vol. 14, Magnetic Tape.

3. Bradshaw, R. L.; Bhushan, B. *ASLE Trans.* **1984**, 27, 33-44.

4. Bradshaw, R. L.; Bhushan, B. *ASLE Trans.* **1984**, 27, 89-100.

5. Bradshaw, R. L.; Bhushan, B. *ASLE Trans.* **1984**, 27, 207-19.

6. Bhushan, B. "Tribology and Mechanics of Magnetic Storage Devices"; Springer-Verlag: New York, 1990.

7. Bradshaw, R.; Bhushan, B.; Kalthoff, C.; Warne, M. *IBM J. Res. Dev.* **March 1986**, 30 (2), 203-15.

8. Dallman H.; Husbach, P. *IEEE Trans. Mag.* **January 1987**, 23 (1), 118-21.

9. Brown, D. W.; Lowry, R. E.; Smith, L. E. "Prediction of the Long Term Stability of Polyester-Based Recording Media". *Natl. Bur. Stand. (U.S.)* **June 1982**, No. 82-2530.

10. "Encyclopedia of Polymer Science and Technology", 2nd ed.; John Wiley and Sons: New York, 1988; Vol. 12, Polyesters, Films.

11. Schollenberger, C. S. In "Polyurethane Technology"; Bruin, P. F., Ed.; John Wiley & Sons: New York, 1969; Chapter 10.

12. Meckel, W., Goyert, W., and Wieder, W. In "Thermoplastic Elastomers, A Comprehensive Review"; Legge, N. R.; Holden, G.; Schroeder, H. E., Eds.; Hanser Publishers: New York, 1987; Chapter 2

13. "Encyclopedia of Chemical Technology", 3rd ed.; John Wiley & Sons:New York, 1983; Urethane Polymers.

14. Seefried, C. G.; Koleske, J. V.; Critchfield, F. E. *J. Appl. Poly. Sci.* **1975**, 19, 2493-502.

15. Seefried, C. G., Koleske, J. V., and Critchfield, F. E. *J. Appl. Poly. Sci.* **1975**, 19, 2503-13.

16. Camberlin, Y., and Pascault, J. P. *J. Poly. Sci., Poly. Chem. Ed.* **1982**, 20, 1445-56.

17. Allport, D. C.; Janes W. H. "Block Copolymers"; Application Science Publishers: London, 1973.

18. "Magnetic Tape and Cartridge for Information Interchange - 18-Track, Parallel, 1/2 inch (12.65 mm), 37 871 cpi (1491 cpmm), Group-Coded - Requirements for Recording". *American National Standards Institute* **1990**, No. X3.180-1990.

19. Bradshaw, R. L. presented at the Association of Canadian Archivists Conference, May 1989.

20. Cudihy, E. F. *IEEE Trans. Mag.* **July 1980**, MAG-16 (4), 558-68.

21. Rodriguez, F. "Principles of Polymer Science", 3rd ed.; Hemisphere Publishing Corporation: New York, 1989.

22. Turi, E. A. "Thermal Characterization of Polymeric Materials"; Academic Press; San Diego, 1981.

23. Wunderlich, B. "Thermal Analysis"; Academic Press: New York, 1990.

24. Ferry, J. D. "Viscoelastic Properties of Polymers"; John Wiley & Sons: New York, 1980.

25. Swalin, R. A. "Thermodynamics of Solids", 2nd ed.; John Wiley & Sons: New York, 1972.

26. Brown, M. E. "Introduction to Thermal Analysis"; Chapman and Hall: New York, 1988.

27. Wendlandt, W. W. "Thermal Analysis"; John Wiley & Sons: New York, 1986.

28. Brennan, W. P.; Norwalk, Conn., March 1978, Perkin-Elmer Thermal Analysis Application Study 24.

29. Lofthouse, M.G.; Burroughs, P. *J. Thermal Analysis* **1978**, 13, 439 - 453.

30. Murayama, T. "Dynamic Mechanical Analysis of Polymeric Material"; Elsevier Scientific Publishing Company: Amsterdam, 1978.

31. Hyver, K.J. "High Resolution Gas Chromatography", 3rd ed.; Hewlett Packard Co., 1989.

32. Feldman, L.C.; Mayer, J.W. "Fundamentals of Surface and Thin Film Analysis"; Elsevier Science Publishing Company: New York, 1986.

33. Wagner, C.D.; Riggs, W.M.; Davis, L.E.; Moulder J.F., "Handbook of X-Ray Photoelectron Spectroscopy"; Perkin-Elmer Corporation, 1979.

34. Goldstein, J.I.; Yakowitz, H.; "Practical Scanning Electron Microscopy"; Plenum Press: New York, 1975.

35. "7 Series/UNIX TGA 7 Thermogravimetric Analyzer Users Manual"; Perkin Elmer Corporation, May 1991.

36. "7 Series/UNIX DSC 7 Differential Scanning Calorimeter Users Manual"; Perkin Elmer Corporation, May 1991.

37. "7 Series/UNIX TMA 7 Thermomechanical Analyzer Users Manual"; Perkin Elmer Corporation, May 1991.

38. "7 Series/UNIX DMA 7 Dynamic Mechanical Analyzer Users Manual"; Perkin Elmer Corporation, May 1991.

39. Stewart, J.E.; "Infrared Spectroscopy Experimental Methods and Techniques"; Marcel Dekker, Inc.: New York, 1970.

40. Jabarin, S. A.; Lofgren, E. A. *Poly. Eng. Sci.* **September 1984**, 24 (13), 1056-63.

41. Cotton, A. F.; Wilkinson, G.; "Advanced Inorganic Chemistry'; Interscience Publishers: New York, 1972.